

# Rates and redshift distributions of high- $z$ supernovae

Tomas Dahlén and Claes Fransson

Stockholm Observatory, 133 36 Saltsjöbaden, Sweden

Received 5 February 1999 / Accepted 26 July 1999

**Abstract.** Using observed star formation rates at redshifts up to  $z \sim 5$ , we calculate cosmic supernova rates for core collapse and Type Ia supernovae. Together with supernova statistics and detailed light curves, we estimate the number of supernovae, and their distribution in redshift, that should be detectable in different filters with various instruments, including both existing and future telescopes, in particular the NGST.

We find that the NGST should detect several tens of core collapse supernovae in a single frame. Most of these will be core collapse supernovae with  $1 \lesssim z \lesssim 2$ , but about one third will have  $z \gtrsim 2$ . Rates at  $z \gtrsim 5$  are highly uncertain. For ground based 8–10 m class telescopes we predict  $\sim 0.1$  supernova per square arcmin to  $I_{AB} = 27$ , with about twice as many core collapse SNe as Type Ia's. The typical redshift will be  $z \sim 1$ , with an extended tail up to  $z \sim 2$ . Detectability of high redshift supernovae from ground is highly sensitive to the rest frame UV flux of the supernova, where line blanketing may decrease the rates severely in filters below  $1 \mu\text{m}$ .

In addition to the standard 'Madau' star formation rate, we discuss alternative models with flat star formation rate at high redshifts. Especially for supernovae at  $z \gtrsim 2$  the rates of these models differ considerably, when seen as a function of redshift. An advantage of using SNe to study the instantaneous star formation rate is that the SN rest frame optical to NIR is less affected by dust extinction than the UV-light. However, if a large fraction of the star formation occurs in galaxies with a very large extinction the observed SN rate will be strongly affected. An additional advantage of using SNe is that these are not sensitive to selection effects caused by low surface brightness.

Different aspects of the search strategy is discussed, and it is especially pointed out that unless the time interval between the observations spans at least 100 days for ground based searches, and one year for NGST, a large fraction of the Type IIP supernovae will be lost. Because of the time delay between the formation of the progenitor star and the explosion, observations of  $z \gtrsim 1$  Type Ia supernovae may distinguish different progenitor scenarios.

A major problem is the determination of the redshift of these faint supernovae, and various alternatives are discussed, includ-

ing photometric redshifts. In practice a reliable classification based on either spectroscopy or light curves requires the SNe to be  $\sim 2$  magnitudes above the detection limit. The uncertainties in the estimates are discussed extensively. We also discuss how the estimated rates depend on cosmology. Finally, some comments on effects of metallicity are included.

**Key words:** cosmology: observations – stars: supernovae: general – stars: formation – nuclear reactions, nucleosynthesis, abundances

## 1. Introduction

The cosmic star formation rate (SFR) has now been estimated up to redshifts  $z \sim 5$ . By combining the evolution of the  $2800 \text{ \AA}$  luminosity density calculated from CFRS-galaxies (Lilly et al. 1996) at redshifts  $z \lesssim 1$ , and the  $1500 \text{ \AA}$  luminosity density calculated from high redshift galaxies ( $z > 2$ ) in the HDF found by the Lyman dropout techniques, Madau et al. (1996) argue that the SFR should peak at  $1 \lesssim z \lesssim 2$ . Complementary to these, Connolly et al. (1997) have used HDF photometric measurements, together with ground based near-IR photometry, to derive the  $2800 \text{ \AA}$  luminosity density at redshifts  $0.5 \lesssim z \lesssim 2$ . These results are in good agreement in the region overlapping with the CFRS, supporting the case of a peak in the SFR. This conclusion is, however, sensitive to the fact that the rest frame light may have been strongly attenuated by dust. Absorption by dust is especially severe for the UV-light, and since shorter rest frame wavelengths are sampled at higher  $z$ , this uncertainty increases with redshift.

The evolution of the SFR is reflected in the cosmic supernova rate (SNR). It should therefore, in principle, be possible to use supernova (from now on SN) observations to distinguish between various star formation scenarios. Even more important, core collapse SNe, i.e. Types II and Ib/c, provide a direct probe of the metallicity production with cosmic epoch. In reality these relations are non-trivial to establish. When it comes to core collapse SNe, the observational constraints at high redshifts are nearly non-existent. Even at low redshift the statistics are severely affected by selection effects. A main problem comes from the fact that core collapse SNe observationally show a

---

Send offprint requests to: T. Dahlén

Correspondence to: tomas@astro.su.se; claes@astro.su.se

large diversity, both in terms of luminosities and types, and with uncertain distributions. In addition, dust absorption, as well as background contamination, affect the statistics. Nevertheless, because of their importance for the nucleosynthesis, as well as galaxy formation, direct observations of the rate of core collapse SNe are of high interest. It is therefore hardly surprising that this is one of the main goals for the Next Generation Space Telescope (NGST) (Stockman 1997).

For Type Ia SNe, the unknown time delay between formation and explosion of the progenitors unties the link to the SFR, making predictions more model dependent. Observations of the Type Ia rate at high redshift therefore provides a possibility to distinguish different progenitor scenarios.

In this paper we present estimates for the expected number of observable SNe for the NGST, as well as for ground based instruments, and discuss various complications entering the analysis. Previous studies include Madau et al. (1998a), Ruiz-Lapuente & Canal (1998), Jørgensen et al. (1997), Miralda-Escudé & Rees (1997), Sadat et al. (1998), Yungelson & Livio (1998). With respect to most of these, our work differs in that we include information about the light curve, as well as spectral evolution, which allow us to predict the simultaneously observable number of SNe. That this is important is obvious from the fact that a nearby SN seen at the tail of the light curve is indistinguishable from a more distant object at the peak. We divide the SNe into different types with maximum absolute magnitudes and spectral distributions that varies with time and type. This also introduces a large dispersion in magnitudes at a given redshift. Neglect of these effects introduces a severe Malmquist bias. We calculate the counts for different broad band filters, and include information about the expected redshift distribution of the detected SNe. Some preliminary results were given in Dahlén & Fransson (1998).

Sect. 2 describes our model. Results are presented in Sect. 3. In Sect. 4 we discuss alternative star formation scenarios. In Sect. 5 we discuss how other cosmologies affect our results. The effects of gravitational lensing are discussed in Sect. 6. Problems concerning redshift determination are discussed in Sect. 7. A general discussion follows in Sect. 8, and conclusions are given in Sect. 9. Throughout most of the paper we assume a flat cosmology with  $H_0 = 50 \text{ km s}^{-1} \text{ Mpc}^{-3}$  and  $\Omega_M = 1$ , unless otherwise stated.

## 2. The model

### 2.1. Filters and magnitude system

Because of the strong UV deficiency in the spectrum of most SN types, filters bluer than R are of little interest for high- $z$  studies. For R ( $\lambda = 0.65 \text{ } \mu\text{m}$ ) and I ( $\lambda = 0.8 \text{ } \mu\text{m}$ ) we use Cousins filters, and in the near-IR J ( $\lambda = 1.2 \text{ } \mu\text{m}$ ) and K' ( $\lambda = 2.1 \text{ } \mu\text{m}$ ) filters. For the M band we use a filter that we denote by M', which is centered on  $\lambda = 4.2 \text{ } \mu\text{m}$  with  $\lambda/\Delta\lambda = 3$ . For the magnitudes we use the AB-system where  $m_{AB} = -2.5 \log F_\nu - 48.6$  (Oke & Gunn 1983) ( $F_\nu$  in  $\text{ergs cm}^{-2} \text{ Hz}^{-1} \text{ s}^{-1}$ ). Here 1 nJy corresponds to  $m_{AB} = 31.4$ . When needed, we have used the

following relations to transform from Vega based magnitudes to AB magnitudes:  $K' = K'_{AB} - 1.84$ ,  $J = J_{AB} - 0.82$ ,  $I = I_{AB} - 0.42$  and  $R = R_{AB} - 0.17$ .

### 2.2. Star formation rates

A problem when using UV-luminosity densities to calculate the SFR is that these can be matched to almost any SFR, ranging from a strongly peaked to a flat, or even increasing, SFR at  $z \geq 1$ , by adjusting the assumed extinction due to dust. By simultaneously using luminosity densities observed in different wavebands it is possible to break this degeneracy. Madau (1998) used three bands (UV, optical and NIR) in order to derive a SFR that can simultaneously reproduce the evolution of the different luminosity densities. He found a best fit for a universal extinction  $E_{B-V}=0.1$  with SMC-type dust. Despite corrections for absorption, the SFR still shows a pronounced peak at  $1 < z < 2$ . This SFR is shown in Fig. 1. A peaked SFR is predicted in scenarios where galaxies form hierarchically (e.g., Cole et al. 1994). Although commonly used, this SFR is not universally accepted and in Sect. 4 we discuss alternative SFR's.

Core collapse SNe, which originate from short lived massive stars (ages  $\lesssim 5 \times 10^7$  yrs), have an evolution that closely follows the shape of the SFR. Assuming an immediate conversion of these stars to SNe renders a multiplicative factor,  $k = \text{SNR}/\text{SFR}$ , between the SFR ( $M_\odot \text{ yr}^{-1} \text{ Mpc}^{-3}$ ) and the SNR ( $\text{yr}^{-1} \text{ Mpc}^{-3}$ ), where  $k$  depends on the IMF and the mass range of the progenitors. Here, we take

$$k = \frac{\int_{8M_\odot}^{50M_\odot} \Phi(M) dM}{\int_{0.1M_\odot}^{125M_\odot} M\Phi(M) dM} \quad (1)$$

Using a Salpeter IMF yields  $k=0.0064$ . Note that, for consistency, the same IMF as assumed when deriving the SFR from the luminosity densities should be used. Using a Scalo IMF, instead of a Salpeter IMF, decreases the conversion factor  $k$  between the SFR and the SNR by a factor 2.6. A Scalo IMF, however, also increases the SFR as derived from the UV luminosities by a factor  $\sim 2$ , hence cancelling most of the effect. The reason is that the same stars that produce the UV luminosities also explode as core collapse SNe.

The lower mass limit for Type II progenitors is generally believed to be 8–11  $M_\odot$  (e.g., Timmes et al. 1996). Here we choose 8  $M_\odot$ , a limit supported by e.g., Nomoto (1984). An increase to 11  $M_\odot$  would decrease  $k$ , and hence the SNR, by  $\sim 38\%$ . Indications from especially the oxygen/iron ratio that the most heavy stars form black holes and do not result in SNe, justifies the use of 50  $M_\odot$  as an upper limit to the progenitor mass (Tsujimoto et al. 1997). Other studies (e.g., Timmes et al. 1995), however, find that stars with masses down to  $\sim 30 M_\odot$  may result in black holes. An upper limit of 30  $M_\odot$ , instead of 50  $M_\odot$ , decreases  $k$  by  $\sim 9\%$ .

The uncertainties concerning the origin of Type Ia SNe makes the relation between the rate of these SNe and the star formation more ambiguous. The predicted SNR depends on the nature of the SN progenitors. Yoshii et al. (1996) argue that the

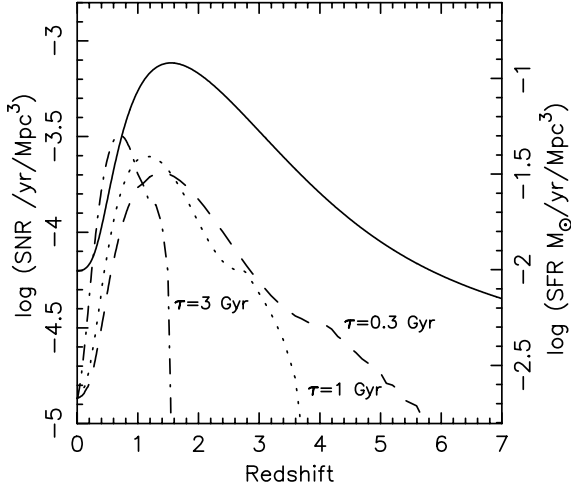


**Fig. 1.** SNRs for the model with dust extinction  $E_{B-V}=0.1$ . The solid line represent the rate of core collapse SNe. This scales directly with the SFR, given by the right hand axis. Dashed, dotted and dash-dotted lines represent the rate of Type Ia SNe with times delays  $\tau=0.3, 1.0$  and  $3.0$  Gyr, respectively. The rates of Type Ia SNe are normalized to fit the locally observed rates.

SNe Ia progenitor lifetime is probably restricted to  $0.5\text{--}3$  Gyr. This range opens a possible way to observationally distinguish between progenitor models. Ruiz-Lapuente & Canal (1998) find that the more short-lived double-degenerate progenitor systems and the long-lived cataclysmic-like systems should yield significantly different rates.

In this paper we use as a standard model the SFRs derived by Madau (1998) to calculate the rates of both core collapse and Type Ia SNe. We use a universal extinction  $E_{B-V}=0.1$ , together with SMC-type dust and a Salpeter IMF. In Sect. 4 we investigate how a higher extinction affects the counts, and if it is possible to use these counts to estimate the amount of dust.

### 2.2.1. Core collapse SNe

The SNR used is shown in Fig. 1. This is the intrinsic rate of exploding SNe, irrespective of magnitudes and spectral distributions. The apparent magnitude of a SN at redshift  $z$  at a time  $t$  off its peak magnitude (i.e.  $t$  can be negative) in a host galaxy with inclination  $i$  observed in a filter  $f$  is given by

$$m_f(z, t, i) = M_f(t) + \mu(z) + K_f(z, t) + A_{g,f} + \langle A_{i,f} \rangle. \quad (2)$$

Here,  $M_f(t)$  is the absolute magnitude of the SN in filter  $f$  at time  $t$  relative to the peak of the light curve,  $\mu(z)$  is the distance modulus,

$$\mu(z) = 5 \log d_L(z) - 5. \quad (3)$$

The luminosity distance,  $d_L$ , is given by,

$$d_L = \frac{(1+z)}{H_0} |\Omega_k|^{1/2} \text{sinn}\{|\Omega_k|^{1/2}\} \times \int_0^z [(1+z)^2(1+\Omega_M z) - z(2+z)\Omega_\Lambda]^{-1/2} dz. \quad (4)$$

**Table 1.** Adopted maximum absolute B magnitudes and dispersion in the AB-system. From Miller & Branch (1990), Cappellaro et al. (1997), Cappellaro et al. (1993) and Patat et al. (1994). Values are corrected for extinction  $E_{B-V}=0.1$ , corresponding to  $A_B=0.32$ . The intrinsic fraction of exploding SNe of the different types are given by  $f$ .

SN Type	$\langle M_{B,0} \rangle$	$\sigma$	$f$
SNIb/c	-18.44	0.39	0.23
SNIIP	-17.86	1.39	0.30
SNIIL	-18.38	0.51	0.30
SN87A-like	-15.43	1.0	0.15
SNIIn	-20.03	0.6	0.02

where  $\Omega_k = 1 - \Omega_M - \Omega_\Lambda$  and ‘sinn’ stands for  $\sinh$  if  $\Omega_k > 0$  and for  $\sin$  if  $\Omega_k < 0$  (Misner et al. 1973). If  $\Omega_k = 0$  then the ‘sinn’ and the  $|\Omega_k|^{1/2}$  terms are set equal to one. For the standard CDM cosmology mainly used here, the distance modulus is given by  $\mu(z) = 45.4 - 5 \log(H_0/50 \text{ km s}^{-1} \text{ Mpc}^{-1}) + 5 \log[(1+z) - (1+z)^{1/2}]$ . Further,  $K_f(z, t)$  gives the K-correction,  $A_{g,f}$  is the Galactic absorption, and  $\langle A_{i,f} \rangle$  is the radially averaged absorption in the parent galaxy with inclination  $i$ .

For Type Ib/c, plateau Type IIP and linear Type IIL SNe we use peak magnitudes given by Miller & Branch (1990). The magnitudes of the faint SN1987A-like SNe are not well known. Here we adopt the magnitudes given by Cappellaro et al. (1993), while magnitudes from Patat et al. (1994) are adopted for the Type IIn SNe. The magnitudes given by these authors are, however, not corrected for absorption. Adopting an average  $E_{B-V} = 0.1$  yields a mean  $A_B = 0.41$  mag. Taking the effect of the albedo of the dust grains into account lowers the effective absorption. We adopt an absorption  $A_B = 0.32$  mag, which is consistent with the mean face-on absorption calculated by Hatano et al. (1998) in their models for Type II SN extinction. We have here assumed that the absorption of the light from the parent galaxy and the SNe follow the same extinction law, implying that the SNe and the progenitor stars occur in the same environment, which to some extent may be incorrect. If the first core collapse SNe and their main sequence progenitors in a region sweeps away part of the shrouding dust, the absorption could be lower than calculated above. In Sect. 4 we return to this possibility. In Table 1 we list the corrected mean absolute B magnitudes, as well as the adopted dispersion in this quantity for the different types at the peak of the light curve.

For the evolution of the luminosity with time we use light curves from Filippenko (1997) for the Type Ib/c’s, IIP’s, IIL’s and the SN1987-like SNe. We have made some modifications to the light curve for the IIP’s to achieve a better fit to the observed, as well as theoretical, light curves presented in Eastman et al. (1994). For Type IIn’s we use a light curve intermediate between IIP and IIL. This seems adequate in view of the data presented by Patat et al. (1994), who find that Type IIn SNe can have both linear and plateau shape, but there are also light curves in-between these two.

The K-correction is calculated by assuming modified blackbodies for the spectral distributions of the SNe. At  $z \gtrsim 1$  even the I-band corresponds to the rest UV part of the spectrum. The exact spectral distribution in the blue and UV is therefore crucial. Unfortunately, this part of the spectrum is relatively unexplored even at low  $z$ . UV observations of Type IIP's are especially scarce. Only for the somewhat peculiar Type IIP SN1987A is there a good UV coverage (Pun et al. 1995). This showed already  $\sim 3$  days after explosion a very strong UV deficit, similar to Type Ia SNe. This is a result of the strong line blanketing by lines from Fe II, Fe III, Ti II and other iron peak elements (e.g., Lucy 1987; Eastman & Kirshner 1989). Although the progenitors of typical Type IIP's probably are red supergiants, rather than blue as for SN1987A, there is no reason why these ions should be less abundant than in SN1987A. On the contrary, because of the near absence of strong circumstellar interaction and similar temperature evolution they are expected to have fairly similar UV spectra, as calculations by Eastman et al. (1994) also show. Eastman et al. find that the UV blanketing sets in after  $\sim 20$  days when the effective temperature becomes less than  $\sim 7000$  K. This coincides with the beginning of the plateau phase. We therefore mimic the UV blanketing by a 2 magnitude drop between  $4000 \text{ \AA}$  and  $3000 \text{ \AA}$ , and a total cutoff short-wards of  $3000 \text{ \AA}$ , for the Type IIP and SN1987A-like SNe with  $T_{eff} \lesssim 7000$  K. At higher  $T_{eff}$  we assume non-truncated blackbodies for these types. The time evolution of the spectra is modeled by changing the characteristic temperature of the blackbody curves to agree with the calculations by Eastman et al. At shock out-break a short interval of energetic UV radiation occurs with  $10^5 \lesssim T_{eff} \lesssim 10^6$  K. This only lasts a few hours, but may due to its high luminosity be observable to high  $z$  (Klein et al. 1979; Blinnikov et al. 1998; Chugai et al. 1999). It then cools to  $\sim 2.5 \times 10^4$  K at  $\sim 1$  day and further to  $\lesssim 7000$  K after  $\sim 20$  days. At the plateau phase the temperature is  $\sim 5000$  K.

From the limited UV information of the Type IIL's SN 1979C, SN 1980K and SN 1985L (Cappellaro et al. 1995), and the Type IIn SN 1998S (Kirshner et al., private communication), we model the spectra of the IIL's and IIn's by blackbody spectra without cutoffs. The most extensive coverage of the UV spectrum of a Type IIL exists for SN 1979C (Panagia 1982). By fitting blackbody spectra to the optical photometry, we find that even after two months, when the color temperature is only  $\sim 6000$  K, there is no indication of UV blanketing. On the contrary, there is throughout the evolution a fairly strong UV excess, consisting of continuum emission as well as lines, in particular Mg II  $2800 \text{ \AA}$ . The UV excess of these SNe is likely to be caused by the interaction of the SN and its circumstellar medium. This ionizes and heats the outer layers of the SN, decreasing the UV blanketing strongly. For the effective temperature as a function of time we use the fits for SN 1979C by Branch et al. (1981). The Type Ib/c light curve is taken from Filippenko (1997) and is assumed to have the same spectral characteristics as the Type Ia (described further below).

The Galactic absorption,  $A_{g,f}$ , is taken to be zero in our modeling. This can easily be changed to other values of  $A_{g,f}$ . The term  $\langle A_{i,f}(z) \rangle$  adds the absorption due to internal dust in

the parent galaxy with inclination  $i$ , according to the adopted extinction laws. Gordon et al. (1997) show that the extinction curve for starburst galaxies lacks the  $2175 \text{ \AA}$  bump, like an SMC-type extinction curve does, and shows a steep far-UV rise, intermediate between a Milky Way and an SMC-like extinction curve. The observed increase with redshift of the UV-luminosity originates mainly from starburst/irregular systems (e.g., Brinchmann et al. 1998). This implies that a major part of the core collapse SNe should be found in such galaxies, and an SMC-type extinction curve should therefore be most appropriate when calculating the absorption of the SNe light. The difference between an SMC-type dust curve and a Milky Way-type extinction in the interesting wavelength range is small. This is especially true for SNe with a short wavelength cutoff in their spectral energy distributions, but also a blackbody spectrum with  $T_{eff} \lesssim 7000$  K drops fast enough at short wavelengths for the precise form of UV absorption in this region to be less important.

The dependence on inclination has been modeled by Hatano et al. (1998). The absorption closely follows a  $(\cos i)^{-1}$  behavior up to high inclinations. We approximate their results by  $\langle A_{B,i} \rangle = 0.32[(\cos i)^{-1} - 1]$ . Also the radial dependence of the absorption is discussed by Hatano et al. We simplify our calculations by adopting their radially averaged value of the absorption. Dividing the host galaxies into different types increases the dispersion in absorption. Finally, the extinction may depend on the intrinsic luminosity and the metallicity of the host galaxy. This variation should to some extent already be accounted for in the observed dispersion of the peak magnitudes.

The SNe are divided into the five different groups, with fractions,  $f$ , representing the intrinsic fraction of exploding core collapse SNe of the different types (i.e. irrespective of magnitude). We estimate  $f$  by using the observed *ratios of discovery*,  $f_{obs}$ , given by Cappellaro et al. (1993), who find  $f_{obs}(\text{IIP}) \simeq f_{obs}(\text{IIL})$ ,  $f_{obs}(\text{Ib/c}) \simeq 0.3 f_{obs}(\text{II})$  and  $f_{obs}(\text{IIn}) \simeq 0.2 f_{obs}(\text{II})$ .

The total number of Type II's is the sum of Type IIP, IIL, 1987A-like and IIn. Adding the Type Ib/c yields the total number of core collapse SNe. Cappellaro et al. (1997) argue that the intrinsic fractions of IIn and 1987A-like should be  $f(\text{IIn}) = (0.02-0.05)f(\text{II})$  and  $f(1987\text{A-like}) = (0.10-0.30)f(\text{II})$ . The IIP, IIL and Ib Types have approximately the same magnitudes, i.e. the ratio of discovery should be close to the intrinsic fractions between these. Combining these values and assumptions leads to our adopted intrinsic fractions in Table 1. We note here that, unfortunately, the rates of the different classes are affected by fairly large uncertainties.

The observable number of SNe with different apparent magnitudes is calculated by integrating the SNR over redshift. The SNe are distributed between the different types according to their intrinsic fractions, and are placed in parent galaxies with inclinations between  $0^\circ$  to  $90^\circ$ . An important feature of our model is that the number of SNe exploding each year are distributed in time, and are given absolute magnitudes consistent with their light curves. With this procedure we obtain the simultaneously observable number of SNe, including both those close to peak and those at late epoch. In order to actually detect the SNe, at least one more observation has to be made after an

appropriate time has passed. In Sect. 8 we discuss the spacing in time between observations.

For  $z > 5$  we use a rate that is an extrapolation from lower  $z$ . This certainly simplifies the actual situation drastically. However, due to the large distance modulus and the decline in the rate at high  $z$ , the fraction of SNe with  $z > 5$  is small, and hence the errors due to the uncertainty in the shape of the SFR at  $z > 5$ . Furthermore, SNe with a spectral cutoff at short wavelengths drop out at redshifts  $z \sim \lambda_{eff}/4000 - 1$ , where  $\lambda_{eff}$  is the effective wavelength of the filter. In the R, I, J, K' and M' filters this occurs at  $z \sim 0.65, 1.0, 2.0, 4.5$  and  $10$ , respectively. This makes the contribution from SNe with higher redshifts insignificant. A caveat here is that lensing, as well as an early epoch of Pop III SNe, may cause a significant deviation from this extrapolation. These issues are discussed in Sect. 4 and Sect. 6.

### 2.2.2. Type Ia SNe

When calculating the number of Type Ia SNe we employ the same procedure as above. We use an extinction corrected peak magnitude  $M_B = -19.99$  and dispersion  $\sigma = 0.27$ , found by Miller & Branch (1990). The time delay between the formation of the progenitor star and explosion of the SNe is treated in a way similar to Madau et al. (1998a). Most likely, the progenitors are stars with mass  $3M_\odot < M < 8M_\odot$  (Nomoto et al. 1994). Stars forming at time  $t'$  reach the white dwarf phase at  $t' + \Delta t_{MS}$ , where  $\Delta t_{MS} = 10(M/M_\odot)^{-2.5}$  Gyr is the time spent on the main sequence. After spending a time  $\tau$  in the white dwarf phase, a fraction  $\eta$  of the progenitors explode as a result of binary accretion at  $t = t' + \Delta t_{MS} + \tau$ . The SNR at time  $t$  can then be written

$$SNR(t) = \eta \int_{t_F}^t SFR(t') dt' \times \int_{3M_\odot}^{8M_\odot} \delta(t - t' - \Delta t_{MS} - \tau) \phi(M) dM, \quad (5)$$

where  $t_F$  is the time corresponding to the redshift of the formation of the first stars,  $z_F$ . Arguments from Yoshii et al. (1996) and Ruiz-Lapuente & Canal (1998) indicate  $0.3 \lesssim \tau \lesssim 3$  Gyr. In the calculations we therefore use three different values for the time delay,  $\tau = 0.3, 1$  and  $3$  Gyr. The  $\tau = 0.3$  Gyr model approximately mimics the double degenerate case, while the  $\tau = 1$  Gyr model resembles the cataclysmic progenitor model. With the additional  $\tau = 3$  Gyr the range is expanded to cover all likely models.

The parameter  $\eta$  in Eq. (6) is introduced to give the fraction of stars in the interval  $3-8 M_\odot$  that result in Type Ia SNe, and is determined by fitting the estimated SNR at  $z = 0$  to the locally observed Type Ia rates. For an alternative approach based on specific assumptions about the progenitors see Jørgensen et al. (1997). Results from local SN searches (Cappellaro et al. 1997; Tammann et al. 1994; Evans et al. 1989) give local rates of 0.12, 0.19, and 0.12 SNU, respectively (1 SNU = 1 SN per century per  $10^{10} L_{B\odot}$ ). Adopting a mean of  $0.14 \pm 0.06$  SNU (Madau et al. 1998a), and using a local B band luminosity estimated by Ellis et al. (1996), leads to a local Type Ia rate of  $1.3 \pm 0.6$

$\times 10^{-5}$  SNe yr $^{-1}$  Mpc $^{-3}$ . The normalization at  $z = 0$  yields an efficiency  $0.04 < \eta < 0.08$ , where the range is due to the fact that different values of  $\tau$  gives different  $\eta$  in order to reproduce the local rates. The uncertainty in the local SNR is equivalent to an additional spread in  $\eta$  by a factor  $\sim 3$ . The normalization to the local rate leads to an uncertainty in the Type Ia SNR at all redshifts that corresponds to the uncertainty in the local rate. This implies an uncertainty by a factor  $\sim 3$  in the estimated Type Ia rates.

The treatment of absorption in the case of Type Ia SNe is more complicated than in the case of core collapse SNe, and is therefore subject to larger uncertainties. The long time delay between the formation of the progenitors and the explosion unties the environmental link between these events. A (binary) star forming in a dusty starburst region may e.g. explode much later as a Type Ia SN in a dust-free elliptical galaxy. Observations show that Type Ia SNe do occur in both elliptical and spiral galaxies. However, the fact that the major part of local Type Ia SNe are detected in spirals, together with observations that indicate that the global fraction of ellipticals, or at least low-dust ellipticals, seems to decrease at increasing redshifts (Driver et al. 1998) may justify our simplification of putting all the SNe Ia in spiral environments. Ignoring the elliptical parent galaxies leads to a slight overestimate of the absorption, and a slight underestimate of the SN detection rate.

Absorption in both the bulge and disk components of spiral galaxies have been calculated by Hatano et al. (1998). They find a somewhat smaller absorption for Type Ia SNe than for core collapse SNe. The Type Ia absorption is also less dependent on the inclination of the parent galaxy. We use the disk component results of Hatano et al. in our model for the absorption of the Type Ia SNe. Fig. 1 show the intrinsic Type Ia SNRs for the three time delays used. Increasing the time delay shifts the peak of the Ia's towards lower redshift. The SFR (and the rate of core collapse SNe) peak at  $z \sim 1.55$ , while the Type Ia rates in the  $\tau = 0.3, 1$  and  $3$  Gyr models peak at  $z \sim 1.35, z \sim 1.16$ , and  $z \sim 0.71$ , respectively.

To describe the spectral energy distribution of the Type Ia SNe we use blackbody curves with a spectral cutoff at  $\sim 4000 \text{ \AA}$  (e.g., Branch et al. 1983). The temperature is set to 15 000 K around the peak, decreasing to 6000 K after  $\sim 25$  days (e.g., Schurmann 1983). We have compared the K-corrections in our model to those calculated from real spectra by Kim et al. (1996). The mean deviation in the R-band correction between our modified black body curves and the detailed calculations by Kim et al. is  $\Delta m \sim 0.1$  mag. This agreement justifies the use of the blackbody representation for the SN spectra. The average Type Ia light curve is taken from Riess et al. (1999).

## 3. Results

Using the model above we can now estimate the observed number of SNe per square arcmin down to some limiting magnitude, including corrections from extinction and the shift of the spectrum with redshift.

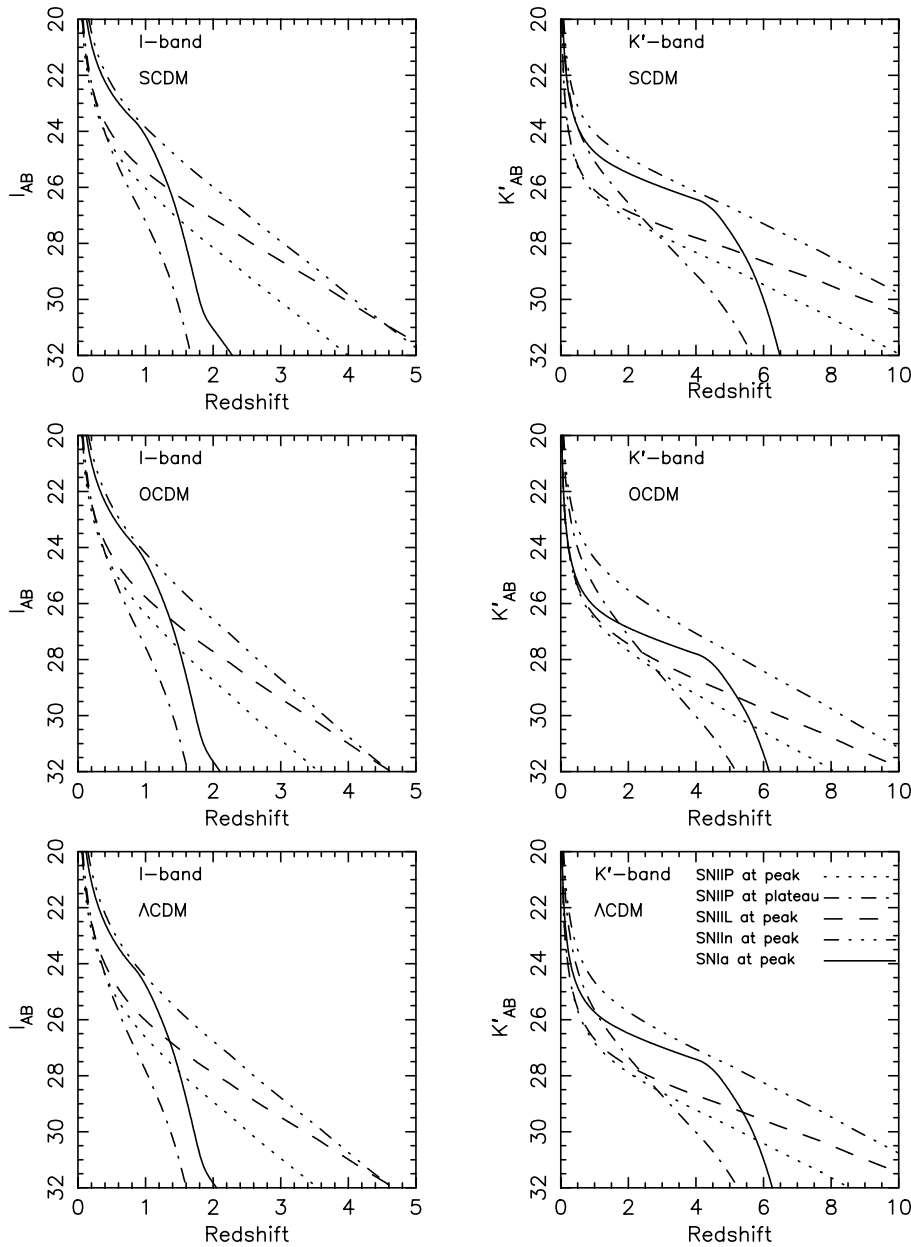


**Fig. 2.** Magnitudes as a function of redshift for different SN types in the I-band (left panels) and the K'-band (right panels). Top panels show SCDM ( $\Omega_M = 1$ ,  $\Omega_\Lambda = 0$ ), middle panels show OCDM ( $\Omega_M = 0.3$ ,  $\Omega_\Lambda = 0$ ) and lower panels show  $\Lambda$ CDM ( $\Omega_M = 0.3$ ,  $\Omega_\Lambda = 0.7$ ). Dotted line shows Type IIP at peak while the dash-dotted line shows the Type IIP at the plateau  $\sim 40$  days after the explosion. Dashed, dash-triple-dot and solid lines show Type IIL, Type IIn and Type Ia, respectively. The magnitude for Type Ib/c's at peak follows the Type Ia's, except for an offset of  $\Delta m \simeq 1.5$  mag towards fainter magnitudes. The magnitude of 1987A-like SNe resembles the Type IIP at the plateau, but with an offset  $\Delta m \simeq 2.0$  towards fainter magnitudes.

As an illustration, we show in Fig. 2 the peak magnitudes (i.e. at  $\sim 10$ – $15$  days after explosion) for Types IIP, IIL, IIn and Ia as a function of redshift. We also show the magnitude of a Type IIP at the plateau phase (age  $\sim 40$  days). The magnitude for Type Ib/c's at peak follows the Type Ia's, except for an off-set of  $\Delta m \simeq 1.5$  mag towards fainter magnitudes. The magnitude of SN1987A-like SNe at the peak resembles the Type IIP at the plateau, but with an off-set  $\Delta m \simeq 2.0$  towards fainter magnitudes. Besides the standard flat  $\Omega_M = 1$  cosmology (hereafter SCDM), we also show the apparent magnitudes for an open cosmology (OCDM) with  $\Omega_M = 0.3$  and  $\Omega_\Lambda = 0$ , and a flat,  $\Lambda$ -dominated cosmology ( $\Lambda$ CDM) with  $\Omega_M = 0.3$  and  $\Omega_\Lambda = 0.7$ . Note that the curves have a dispersion in magnitude according to values given in Table 1. The dispersion is largest for the Type IIP's; the peak magnitude of these may vary by more than one

magnitude. Fig. 2 shows that the Type Ia's and the Type IIP's at the plateau drop out of the I and K'-band at  $z \sim 1$  and  $z \sim 4.5$ , respectively, as a result of their UV-cutoffs. In contrast, the UV-bright Type IIL's and IIn's stay relatively bright in the I band even at high  $z$ .

### 3.1. Core collapse rates

The solid lines in Fig. 3 show the number of predicted core collapse SNe per square arcmin in the R, I, K' and M' filters for different limiting AB-magnitudes. Because of the drop in the UV flux, bands bluer than R are of less interest for high redshifts.

According to the specifications, NGST should have a detection limit of  $\sim 1$  nJy in the J and K' bands and  $\sim 3$  nJy in

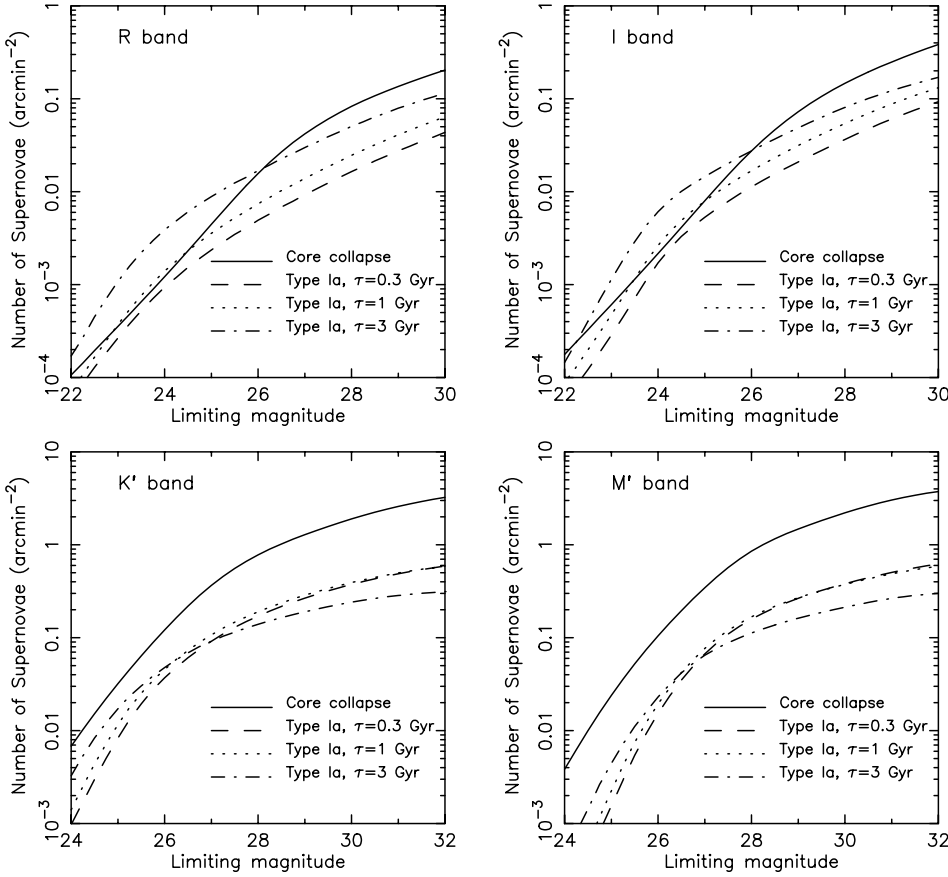


**Fig. 3.** Number of SNe per square arcmin that can be detected down to different limiting magnitudes in the R, I, K' and M' bands. Solid lines represent core collapse SNe. Dashed, dotted and dash-dotted lines represent Type Ia SNe with time delays  $\tau=0.3$ , 1 and 3 Gyr, respectively. Note that AB-magnitudes are used.

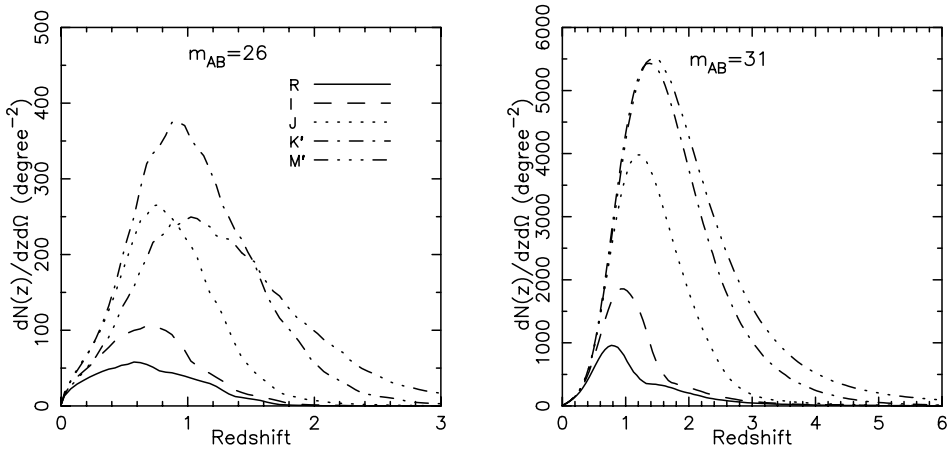


**Fig. 4.** Redshift distribution of core-collapse SNe in the R, I, J, K' and M' filters for limiting magnitudes  $m_{AB}=26$  (left panel) and  $m_{AB}=31$  (right panel).

the M' band for a  $10^4$  s exposure with  $S/N=10$  and  $\lambda/\Delta\lambda = 3$  (Stockman 1997). These fluxes correspond to AB magnitudes of  $J_{AB} = 31.4$ ,  $K'_{AB} = 31.4$  and  $M'_{AB} = 30.2$ , respectively. Using these limits, we find that the K' band yields the highest number of core collapse SNe. In a  $4 \times 4$  square arcmin field we predict  $\sim 45$  simultaneously detectable core collapse SNe, with a mean redshift  $\langle z \rangle = 1.9$ .

In Fig. 4 we show the redshift distribution in all bands for  $m_{AB} = 26$  and  $m_{AB} = 31$ . For the lower magnitude limit one clearly sees the advantage of the infrared J, K' and M' bands when it comes to detect SNe with  $z \gtrsim 1$ . This is, of course, even more pronounced for  $m_{AB} = 31$ , with the M' band having the

highest number of SNe at  $z \gtrsim 2$ . Note, however, that reaching  $R_{AB} \sim 26$  is considerably easier than  $J_{AB}$  or  $K'_{AB} \sim 26$  from ground. The smaller detector size in the latter bands is also a severe limiting factor.

For SNe with redshifts  $z > 5$  we estimate  $\sim 1$  SN per NGST field in the M' filter. The actual numbers of the high- $z$  SNe are highly uncertain, since the SNR at  $z > 5$  is based on an extrapolation from lower redshifts. Also gravitational lensing may be important at these redshifts (see Sect. 6). However, independent of the actual numbers, we find that the M' filter yields a factor  $\gtrsim 2$ –5 higher counts compared to the K' filter at these redshifts.

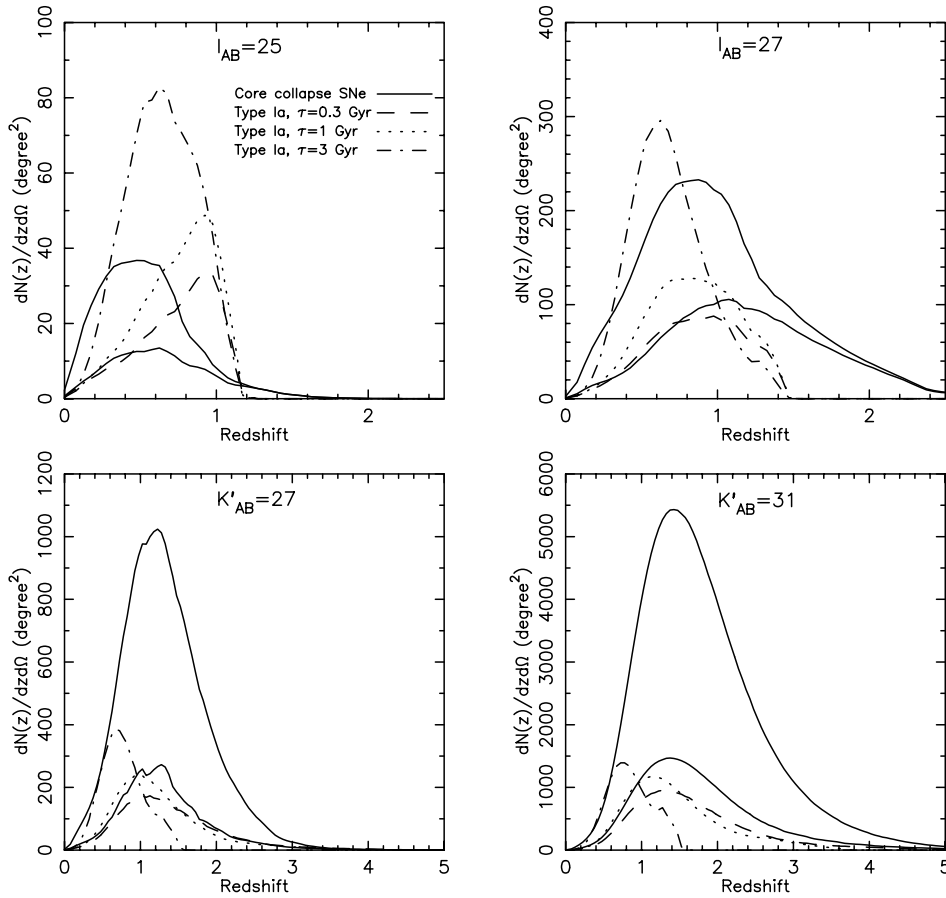


**Fig. 5.** Top panels: Observed SN distribution in redshift in the I filter, for limiting magnitudes  $I_{AB}=25$  and  $I_{AB}=27$ . Upper solid lines show the total number of core collapse SNe, while the lower solid lines show the part originating from Type IIL and Type IIn SNe, i.e. the SNe without a UV cutoff in their spectra over the whole light curve. Dashed, dotted and dash-dotted lines show the number of Type Ia SNe for models with  $\tau=0.3$ , 1 and 3 Gyr, respectively. Bottom panels: Same for  $K'$  filter with limiting magnitudes  $K'_{AB}=27$  and  $K'_{AB}=31$ . Note the expanded redshift scale in the  $K'$  band, as well as the different scales of the y-axis.

We also find that NGST should be well suited to detect SNe originating from a possible Pop III at redshifts  $\gtrsim 10$ .

The R and I bands sample light with rest wavelengths shortward of the peak in the blackbody curves at lower redshifts than the J,  $K'$  and  $M'$  bands do. Besides the drop in luminosity due to the spectral shape (an effect especially pronounced for SNe with strong UV blanketing), these wavelengths are affected by larger extinction. The large K-correction decreases the rates in the R and I bands, and few SNe with  $z \gtrsim 1$  are detected in I and R, even for limiting magnitudes  $\gtrsim 29$ . Increases in these bands are instead caused by sampling SNe with fainter absolute magnitudes at  $z \lesssim 1$ .

In Fig. 5 we show the redshift distribution of core collapse and Type Ia SNe down to  $I_{AB} = 27$  and  $K'_{AB} = 31$ , respectively. The total number of core collapse SNe is shown as the solid lines in each panel. The lower solid line shows the fraction of these coming from Type IIL and Type IIn SNe, which lack UV-cutoff in their spectrum over the whole light curve. The  $I_{AB} = 27$  panel clearly demonstrates the dominance of these at high redshift. Besides these, only the fraction of Type IIP's which are seen near the peak, before UV blanketing sets in, contribute to the SNe with  $z \gtrsim 1.5$ . The  $K'$  band is far less sensitive to this effect, since the UV cutoff does not affect this filter at  $z \lesssim 4.5$ . When we compare the redshift distribution for  $K' = 27$  and  $K' = 31$ , we note that the mean redshift does not change much. However, the absolute number increases by a factor  $\sim 5$ . This is mainly

caused by SNe below the light curve peak. Also the number of high redshift SNe with  $z \gtrsim 2$  increases by a large factor.

Table 2 gives some examples of our estimates for the number of SNe for NGST, VLT/FORS and HST/WFPC2, all for an exposure of  $10^4$  s and  $S/N = 10$ . For VLT/ISAAC and HST/NICMOS the small field and the relatively bright limiting magnitudes, compared to NGST, do not result in more than  $\sim 0.01$  SNe per field. These instruments are therefore of limited interest when it comes to detecting high- $z$  SNe.

So far we have discussed the number of SNe that are simultaneously observable during one search. To actually detect the SNe, additional observations are obviously required. Preferentially, a series of observations of each field should be undertaken in order to obtain a good sampling of the light curves. This also leads to the detection of new SNe in the additional frames. The number of new SNe depends on the total length of the search, and the spacing in time between each observation. As an illustration, in an idealized situation where a field is covered continuously during one year, the detected number of SNe per square degree, with limit  $I_{AB} = 27$ , is increased from  $\sim 260$  in the first image, to  $\sim 1650$  for the whole years coverage. This procedure is, of course, observationally unrealistic. Using 80 days between each observation (i.e.  $\sim$  five observations for a years coverage) results in a total of 1150 different SNe. Using 40 days instead ( $\sim$  ten observations) gives  $\sim 1400$  different SNe. Due to the time

dilatation factor  $(1+z)$ , one observes relatively fewer new SN explosions at high redshifts compared to the first detection.

With NGST, using limits as above, we estimate  $\sim 45$  SNe in each frame. The total number of different SNe in a field that is covered continuously during one year is  $\sim 68$ . This means that in addition to the  $\sim 45$  SNe observed in the first field, only  $\sim 23$  new SNe have exploded during the year. With three observations and 180 days between the observations,  $\sim 63$  different SNe are detected.

Compared to earlier estimates, our use of complete light curves during the whole evolution, as well as distribution of the SNe over time, results in a larger number of SNe, as well as a realistic distribution over redshift for a given magnitude. For example, with the same SFR and extinction, Madau et al. (1998a) predict  $\sim 7$  SNe per NGST field per year in the range  $2 < z < 4$ . Our calculations result in  $\sim 22$ . The difference is due to the fact that we use light curves covering the whole evolution, which allow us to include SNe at all epochs, instead of only those at peak, which is the case in Madau et al.

### 3.1.1. Shock breakout supernovae

Chugai et al. (1999) have noticed that the short peak in the light curve connected with the shock breakout may give rise to a transient event with a duration of a few hours. The possibility to observe this was pointed out already by Klein et al. (1979), although they concentrated mainly on the soft X-ray range.

Based on a radiation-hydrodynamics code, similar to that of Eastman et al. (1994), Chugai et al. have calculated monochromatic light curves for a Type IIP SN (or rather a scaled SN 1987A model) and a Type IIb (specifically SN1993J). With a short time interval between observations these SNe will be easily distinguishable from the Type Ia and Ib/c SNe, which have a rise time of  $t \gtrsim 20$  days (at  $z \gtrsim 1$ ), and therefore only show a modest change in luminosity. A major problem in comparing their results to ours is that it is not discussed how they obtain their adopted intrinsic SNR's, although they approximately agree with those used in this paper, as well as Madau (1998). They also neglect dust extinction in their calculations.

Using this model, Chugai et al. find that two deep exposures, separated by  $\sim 10$  days, result in 1.3 Type II SNe in the  $6.8 \times 6.8$  square arcmin field of the VLT/FORS camera, using limit  $I_{AB} = 28.2$ . In the calculations Chugai et al. assume that all SNe with  $z \leq 2$  are detected with this limit.

Using our hierarchical model, which gives approximately the same SNR up to  $z \sim 2$ , and the same observational set-up, as Chugai et al., our calculations result in  $\sim 0.27$  SNe. The reason for our lower estimate is that Chugai et al. assume all Type II SNe to have the same steep initial rise as the Type IIP and IIb. In our model we do not include any shock breakout for Types IIL and IIn, since the early time behavior of these SN types is not well known. If we do include all Type II SNe, our estimate increases to 0.66 SNe. The remaining discrepancy is mainly caused by the simplification Chugai et al. do by assuming that all SNe with  $z \leq 2$  are detected, combined with the fact that they do not include dust extinction in their calculations.

Nevertheless, this may be an interesting way of studying the shock breakout of SNe. Unfortunately, it may be difficult to estimate the temperature and luminosity separately from this type of observations, because most of the observed evolution will be in the Rayleigh-Jeans part of the spectrum. Soft X-rays, as proposed by Klein et al., is here a better probe.

### 3.2. Type Ia SNe

Fig. 3 shows that in the R and I bands the number of core collapse SNe is comparable or larger than the number of Type Ia SNe for magnitudes fainter than 25–26. The exact crossing point depends on the life time of the SN Ia progenitors, as well as the Type Ia normalization at low  $z$ . In the  $K'$  and  $M'$  bands core collapse SNe tend to dominate at all magnitudes. The reason for this difference is that the Type Ia SNe have a higher effective temperature over a longer period than the Type II SNe. The optical to IR flux ratio is therefore higher for the Type Ia's.

To illustrate the dependence on the progenitor life time, Fig. 3 gives the number of Type Ia SNe for  $\tau = 0.3, 1$  and 3 Gyr in the different filters. Fig. 3 shows that a change in the progenitor life time,  $\tau$ , introduces a non-negligible variation in the predicted number of observable SNe. For example, with an NGST detection limit,  $K'_{AB} = 31.4$ , we predict  $\sim 8$  SNe for the two low values of  $\tau$ , and  $\sim 5$  for  $\tau = 3$  Gyr. Observations in the I band with limits and field as for the VLT/FORS (see Table 2) results in 0.8, 1.1, and 1.8 SNe for increasing values of  $\tau$ . Counts may therefore seem like a useful probe to distinguish between different progenitor models (Ruiz-Lapuente & Canal 1998). However, the uncertainty in the modeling, especially in the normalization of the Type Ia rates to the local value, makes the counts highly model dependent. In next section we show that this is further hampered by the additional dispersion introduced when considering alternative star formation and extinction models.

If both SN type and redshift information are available for the observed SNe, it may be possible to use the redshift distribution of the SNe to distinguish between progenitor scenarios. Figs. 1 and 5 show that the peak in the SNR moves to lower  $z$  as  $\tau$  increases. Also, the high redshift cutoff in the rates depends strongly on  $\tau$ . Fig. 1 shows that the rates decrease towards zero at redshifts  $z \sim 5.5$ ,  $z \sim 3.5$  and  $z \sim 1.5$ , for models with  $\tau = 0.3$  Gyr,  $\tau = 1$  Gyr and  $\tau = 3$  Gyr, respectively. To reach these redshifts, filters unaffected by the UV cutoff must be used (i.e.,  $\lambda_{eff} \gtrsim 4000(1+z) \text{ \AA}$ ). Fig. 5 shows that the I filter is insensitive to Type Ia's at  $z \gtrsim 1.5$ , due to the spectral cutoff. Using the  $K'$  filter (lower panels of Fig. 5) makes it possible to sample all types of SNe up to  $z \sim 5$ , which is therefore most suitable for distinguishing different progenitor models. As already mentioned, this requires a determination of both SN type and redshift. A discussion of methods and problems regarding this follows in Sect. 7.

The only observational estimate of a Type Ia SNR at moderate redshift is by Pain et al. (1996). From a careful analysis, using realistic light curves and spectra, they find a Type Ia rate at  $z \sim 0.4$  of  $34.4^{+23.9}_{-16.2} \text{ SNe yr}^{-1} \text{ deg}^{-2}$  for  $21.5 < R_{AB} <$

**Table 2.** Estimated number of SNe per field for different instruments. The limiting magnitudes are given for a  $10^4$ s exposure and  $S/N=10$ .

Instrument	Field (arcmin <sup>2</sup> )	Filter	limit ( $m_{AB}$ )	Core collapse			Type Ia ( $\tau=1$ Gyr)		
				N(tot)	N( $z > 1$ )	N( $z > 2$ )	N(tot)	N( $z > 1$ )	N( $z > 2$ )
NGST	16	M'	30.2	37	33	15	6.3	4.8	1.2
NGST	16	K'	31.4	45	40	16	8.5	6.5	1.6
NGST	16	J	31.4	27	22	5	6.3	4.4	0.6
VLT/FORS	46	I	26.6	2.4	0.9	0.05	1.1	0.3	-
VLT/FORS	46	R	26.8	1.6	0.7	0.03	0.57	0.03	-
HST/WFPC2	5	I	27.0	0.36	0.16	0.02	0.15	0.05	-
HST/WFPC2	5	R	27.5	0.30	0.15	0.02	0.09	0.01	-

22.5. Using the same magnitude interval, and counting the SNe exploding during one year, we find  $5\text{--}24$  SNe  $\text{yr}^{-1} \text{deg}^{-2}$  for  $\tau = 0.3\text{--}3$  Gyr, where the lower number corresponds to the  $\tau = 0.3$  Gyr model. The mean redshift of these SNe is in our calculation  $\langle z \rangle \sim 0.35$ . These results seem to agree well, possibly favoring a high value of  $\tau$ . Note, however, that our estimated rate of Type Ia's is highly dependent on the normalization set by the local rate of these SNe (i.e., the efficiency parameter  $\eta$ ). We have already seen that the uncertainty in this normalization may be a factor  $\sim 3$ .

### 3.2.1. Number of pre-maximum Type Ia SNe

The number of simultaneously detectable SNe discussed above is a result of events over the whole light curve. Using Type Ia's as standard candles for determination of  $\Omega_0$  requires observations at the peak of the light curve, i.e. that a first detection is made at the rising part of the light curve. We estimate the number of such SNe by assuming that the comoving rise time is 15 days. Fig. 6 shows the number of Type Ia SNe down to different limiting magnitudes before the peak of the light curve in the I filter for the three values of  $\tau$ . Also shown is the number of such SNe with  $z > 1$  (the lower sets of curves). An I band survey covering a one square degree field with limiting magnitude  $I_{AB} \sim 27$ , will detect 16–31 pre-maximum Type Ia SNe (lower numbers for lower values of  $\tau$ ), corresponding to  $\sim 30\%$  of the total number. About 5–8 of the pre-maximum Type Ia's have redshifts  $z > 1$ . These numbers are, again, sensitive to the local rate of Type Ia SN.

## 4. Alternative star formation scenarios

### 4.1. High extinction models

There are several claims that an extinction  $E_{B-V}=0.1$ , as estimated by Madau (1998) and used here, is too low. Meurer et al. (1997) use the ratio between the far-IR and UV fluxes as a probe of the dust extinction in a galaxy, and find that the high redshift UV dropout galaxies may have a UV absorption of 2–3 mag. Using ISO observations of the HDF, Rowan-Robinson et al. (1997) estimate that only a third of the star formation is revealed by the UV-luminosity, with the rest shrouded by dust. Observations with SCUBA at  $850 \mu\text{m}$  (Hughes et al. 1998; Smail et al. 1997) also indicate that a large fraction of the early

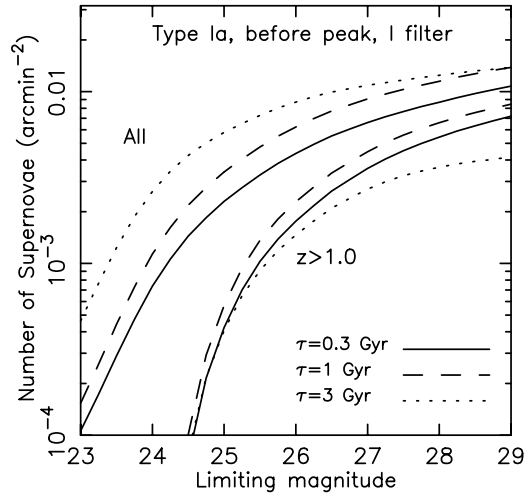


**Fig. 6.** The number of simultaneously detectable Type Ia SNe on the rising part of the light curve for the I filter for three different values of  $\tau$ . Upper sets of curves show the total number of SNe, while the lower sets show SNe with  $z > 1$ .

star formation is hidden by dust. Several other estimates, based on observations of high- $z$  galaxies (eg. Sawicki & Yee 1998; Ellingson et al. 1996; Soifer et al. 1998), support a higher extinction of  $E_{B-V} \sim 0.3$ . Observations of the far-infrared extragalactic background (Burigana et al. 1997) also seem consistent with a higher extinction.

With an extinction of  $E_{B-V} \sim 0.3$  it is likely that the observed peak in the SFR derived from UV-luminosities is illusive, and that the star formation history is compatible with a more constant rate, as in a monolithic collapse scenario (e.g., Larson 1974; Ortolani et al. 1995). In this model galaxy formation is thought to have occurred during a relatively short epoch at high redshift,  $z_F \gtrsim 5$ . This yields a SFR that increases from  $z = 0$  to  $z \sim 1.5$  and then stays almost constant up to  $z \gtrsim 5$ . A SFR of this form may be compatible also with a hierarchical model, as shown in a recent paper by Somerville & Primack (1998).

It should be noted that although there is much in favor for models with a flat SFR to  $z \gtrsim 5$ , they tend to over-predict the metallicity in the region  $z \simeq 2\text{--}3$ , compared to estimates from damped Lyman- $\alpha$  systems (Blain et al. 1999; Madau et al. 1998b; Pei et al. 1998). These models also seem to over-predict the local K-band luminosity (Madau et al. 1998b).

We have calculated the SFR and the resulting SNRs for this high dust scenario by adjusting the observed UV luminosities of Lilly et al. (1996) and Madau (1998) to an extinction  $E_{B-V}=0.3$ . We also increase the local SFR in this model so that the observed B band luminosity density of Ellis et al. (1996) is reproduced. The onset of star formation is set to  $z_F=5$ , while at even higher redshifts the SFR declines quickly. In Sect. 4.3 we comment on how higher values of  $z_F$  affect the estimated rates. For the normalization of the type Ia's at  $z=0$ , we assume that the increase in the intrinsic local B-band luminosity density should lead to an increase in the Type Ia rate by approximately the same amount. In Fig. 7 we show this SFR and the intrinsic SNR for both core collapse SNe and Type Ia SNe, assuming  $\tau=1$  Gyr (dashed lines).

#### 4.2. Low extinction models

The model above combines a high star formation at high redshifts with a high extinction in order to match the same observed luminosity densities. Another alternative scenario is an increased SFR at high  $z$ , but a low extinction, as in the original hierarchical model. Evidence for such a scenario come from Pascarelle et al. (1998), who calculate the evolution of the UV luminosity density up to  $z \sim 6$  from  $\sim 1000$  galaxies with photometric redshifts in the HDF. Taking the effects of cosmological surface brightness dimming into account and using a limiting surface brightness independent of redshift, they argue that the claimed UV luminosity density decrease at  $z > 2$  is mainly caused by a selection effect. Further, Hu et al. (1998) show that an increasing fraction of the total SFR at high redshift takes place in Ly $\alpha$  emitters, and find that the fraction at  $z \sim 3$  may be comparable to that derived from the dropout galaxies. Most of these objects would not show up in a survey such as the HDF, due to their low surface brightness. There is, however, no reason why SNe in these galaxies should not be detectable, especially since the authors argue that the extinction in these objects should be low.

To mimic this scenario we have constructed a SFR with low extinction,  $E_{B-V}=0.1$ , that increases like the hierarchical model up to  $z \sim 1.5$ , but stays flat at higher redshifts up to a formation redshift,  $z_F=5$ . The normalization of the Type Ia's at  $z=0$  is the same as in the hierarchical model. This SFR and corresponding SNRs are shown in Fig. 7 as the dotted line.

#### 4.3. Results for alternative dust and star formation models

We have repeated our calculations in Sect. 3 for the two additional scenarios described above. In the optical filters (probing rest-frame UV to optical), the increased SFR in the high dust model is mostly compensated for by higher extinction, resulting in observed rates that are only  $\sim 10\%$  above those in the hierarchical scenario. The NIR filters (probing rest-frame optical to NIR) are less affected by extinction, which leads to a factor  $\sim 2$  higher rates in the high dust model, compared to the hierarchical model. The estimates differ even more when comparing high redshift subsamples, i.e. when  $z \gtrsim 2$  is observed. This

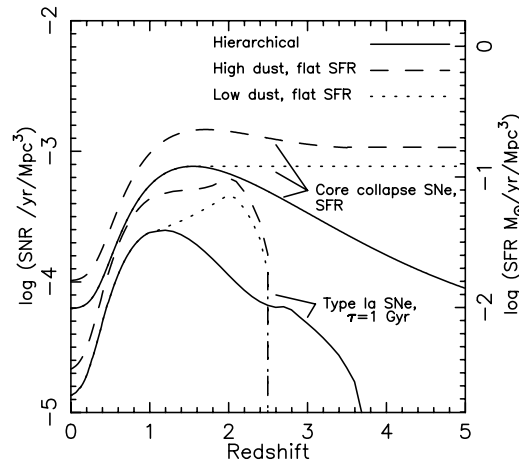


**Fig. 7.** Intrinsic SNRs for the three different models. Solid lines show the hierarchical model with  $E_{B-V}=0.1$ , dashed lines show the high dust model with  $E_{B-V}=0.3$  and flat SFR at high  $z$ , and dotted lines show the model with  $E_{B-V}=0.1$  and a flat SFR at high  $z$ . Upper lines show the rates of core collapse SNe. These scale directly with the SFR, given on the right axis. Lower lines show the rate of Type Ia, for  $\tau=1.0$  Gyr model for each of the SFR models.

illustrates that the observed SNR may serve as an independent probe for the instantaneous SFR that is not subject to the same high uncertainty due to the unknown amount of dust extinction as the UV-luminosity is.

For comparatively bright limiting magnitudes, that do not probe SNe above the proposed peak in the hierarchical scenario, the two models with  $E_{B-V}=0.1$  give, by construction, the same result. Observations must reach SNe at  $z \sim 2$  before the rates start to differ.

Except for the rare Type II's, a SN at peak magnitude at  $z \sim 2$  has  $K'_{AB} \gtrsim 27$ , making NGST necessary for this type of observations. As an illustration, Table 3 shows to what extent rates of core collapse SNe are useful to constrain the SFR at high redshifts. For core collapse SNe with  $z \gtrsim 2$ , NGST should detect  $\sim 3$  and  $\sim 2$  times higher rates for the high-dust-flat-SFR model and the low-dust-flat-SFR model, respectively, compared to the hierarchical model. At  $z \gtrsim 4$  these factors are  $\sim 5$  and  $\sim 4$ .

Due to the short time interval between formation and explosion in the case of core collapse SNe the choice of formation redshift enters only for observations that are deep enough to actually probe  $z_F$ . Table 3 shows the variation of the estimated number of core collapse SNe with  $z > 5$  in the two models with flat SFR as  $z_F$  is changed from  $z_F=5$  to  $z_F=7$  and  $z_F=10$ . Note that more than 10% of the SNe in the M' band have a redshift  $\gtrsim 5$  in these models, compared to  $\sim 2\%$  in the hierarchical model.

Our calculations show a modest increase in the number of Type Ia's for the high dust scenario, compared to the hierarchical scenario, at magnitudes brighter than  $\sim 25$ . At magnitudes corresponding to  $z \gtrsim 1$ , the differences are considerably larger. This is also true for the scenario with flat high- $z$  SFR and low extinction, but the increase is modest, and it does not start be-

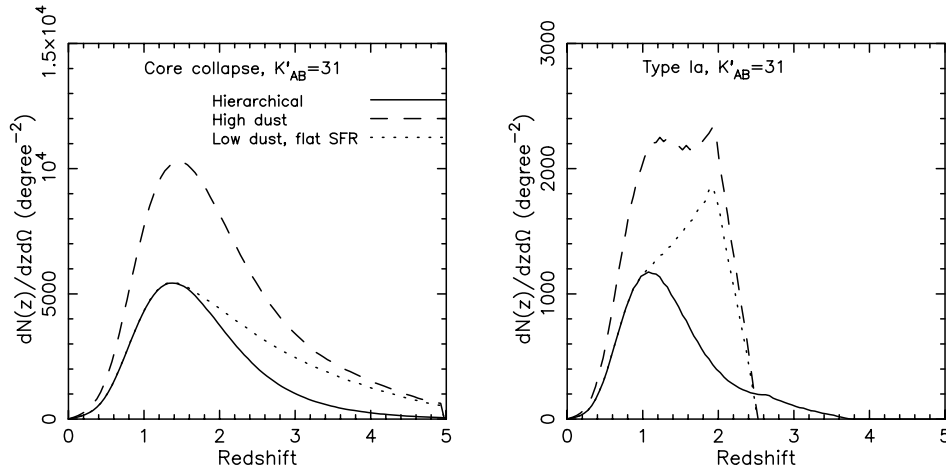


**Fig. 8.** Redshift distribution for core collapse and Type Ia SNe observed to  $K'_{AB}=31$  for the three different SFR models. Results for core collapse SNe are shown in the left panel, while the right panel shows the results for Type Ia SNe with  $\tau=1.0$  Gyr. Note the different scales on the y-axis.

**Table 3.** Estimated number of core collapse SNe per sq. arcmin in the  $M'$  and  $K'$  band for different SFR and dust models.  $N(\text{tot})$  gives the total number of SNe, while the other columns gives the number of SNe with a redshift above different specified values. The two models with flat SFR at high  $z$  has a formation redshift  $z_F = 5$ , except in the two rightmost columns where the formation redshift is set to  $z_F = 7$  and  $z_F = 10$ , respectively.

Model	$E_{B-V}$	Limit $m_{AB}$	$N(\text{tot})$	$N(z > 1)$	$N(z > 2)$	$N(z > 4)$	$N(z > 5)$	$N(z > 5)$ $z_F = 7$	$N(z > 5)$ $z_F = 10$
Hierarchical	0.1	$M'=30$	2.2	1.9	0.85	0.11	0.05	0.05	0.05
		$K'=31$	2.6	2.2	0.86	0.06	0.02	0.02	0.02
High dust, flat SFR	0.3	$M'=30$	6.6	6.0	3.6	0.72	-	0.75	1.0
		$K'=31$	5.8	5.2	2.6	0.29	-	0.15	0.20
Low dust, flat SFR	0.1	$M'=30$	3.2	2.9	1.9	0.42	-	0.44	0.63
		$K'=31$	3.5	3.1	1.7	0.25	-	0.14	0.20

fore  $z \sim 1.5$ . As an illustration, Fig. 8 shows for the  $\tau = 1$  Gyr model that for  $K'_{AB} \lesssim 31.4$ , the number of Type Ia SNe increases by a factor  $\sim 2$  for the two models with flat SFR at high  $z$ , compared to the hierarchical model. Including the full range of  $\tau$  and different star formation scenarios, the NGST should detect between 5–25 Type Ia SNe per field in the  $K'$  band. For the ground based limit,  $I_{AB} = 27$ , the number of Type Ia SNe increases by a factor 1.4–1.9 for the high dust scenario, and a factor 1.0–1.8 for the low dust scenario with flat SFR (smaller increase for lower values of  $\tau$ ).

If  $\tau$  is long, stars formed at early cosmological epochs may survive until low redshifts before ending as Type Ia SNe. Therefore, the increased star formation at high redshifts in the two constant SFR models makes the rate of Type Ia SNe sensitive to the assumed formation redshift,  $z_F$ . The choice of  $z_F$  affects the SNR down to a redshift  $z$ , corresponding to a time  $t = t_F + \Delta t_{MS} + \tau$ . Increasing  $z_F$  to  $> 5$  increases the rates at  $z \gtrsim 2.7$ ,  $z \gtrsim 2.0$  and  $z \gtrsim 1.0$  for  $\tau = 0.3, 1$  and 3 Gyr, respectively. For example, with  $\tau = 1$  Gyr the high- $z$  cutoff in the Type Ia rate occurs at  $z \sim 2.5$  for the two models with flat SFR and  $z_F = 5$  (see Fig. 7). With  $z_F = 7$  and  $z_F = 10$  the cutoff in the rates moves to  $z \sim 3.0$  and  $z \sim 3.4$ , respectively. This effect is larger for smaller values of  $\tau$ .

As earlier mentioned, a further possibility that may increase the predicted counts of core collapse SNe is if the first SNe and

their progenitors sweep away the dust, making the extinction lower for a large fraction of the SNe relative to the stars that produce the UV luminosity. We have studied this scenario by simply neglecting the extinction of the SNe in the two models with  $E_{B-V} = 0.1$  (not included in Table 3). The main difference occurs for the optical bands, where the effect of a lower extinction is largest. In the I band the counts increase by a factor  $\sim 2$ , whereas the counts increase by a factor  $\sim 1.4$  in the  $K'$  band for limits  $K'_{AB} \lesssim 27$ . At fainter  $K'$  limits, i.e. reaching beyond the peak region, the differences decrease because a majority of all SNe is detected in both models, despite the different amount of absorption. For  $K'_{AB} = 31.4$  the increase is therefore only  $\sim 10\%$ .

## 5. Dependence on cosmology

Besides the standard flat  $\Omega_M = 1$  cosmology (SCDM) used so far, we have also studied two additional cosmologies; one open cosmology (OCDM) with  $\Omega_M = 0.3$  and  $\Omega_\Lambda = 0$ , and one flat,  $\Lambda$ -dominated cosmology ( $\Lambda$ CDM) with  $\Omega_M = 0.3$  and  $\Omega_\Lambda = 0.7$ . The most obvious effect of a different cosmology comes from the luminosity distance,  $d_L$  (Eq. (5)). Changing from SCDM to OCDM and  $\Lambda$ CDM increases the distance modulus, making the high- $z$  SNe fainter (Eqs. (4) & (5)), as seen in Fig. 2. The increased distance modulus in the OCDM and  $\Lambda$ CDM cosmologies also affects the intrinsic star formation rates used. A larger

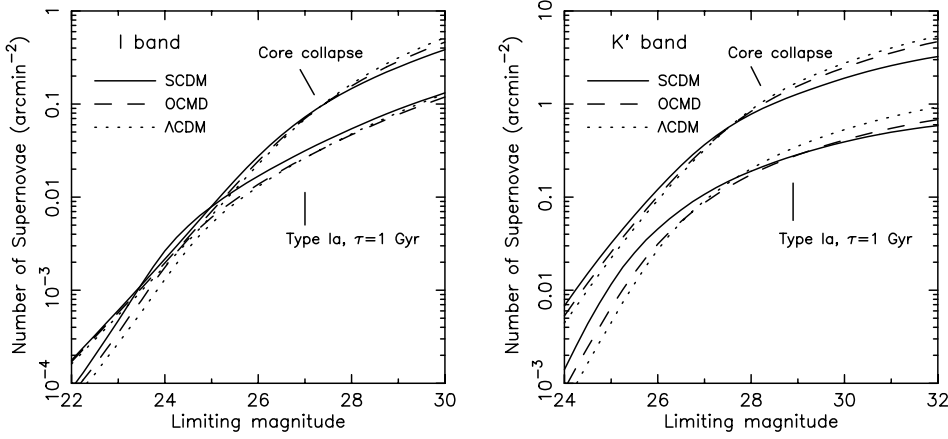


**Fig. 9.** Number of SNe per square arcmin that can be detected down to different limiting magnitudes in the I and  $K'$  bands for three different cosmologies; SCDM ( $\Omega_M = 1$ ,  $\Omega_\Lambda = 0$ ), OCDM ( $\Omega_M = 0.3$ ,  $\Omega_\Lambda = 0$ ) and  $\Lambda$ CDM ( $\Omega_M = 0.3$ ,  $\Omega_\Lambda = 0.7$ ). For the Type Ia rates we assume a delay time  $\tau = 1$  Gyr.

distance modulus implies an increase in the absolute magnitudes of the galaxies from which the star formation rate, and hence also the supernova rates, are derived. As expected, these two effects, i.e. fainter apparent SNe and an increased SNR, almost cancel when it comes to the observed number of core collapse SNe per square angle.

The cosmology also affects the volume element, given by

$$dV = \frac{d_M^2}{(1 + \Omega_k H_0^2 d_M^2)^{1/2}} d(d_M) d\Omega, \quad (6)$$

where  $d_M$  is the proper motion distance,  $d_M = (1+z)^{-1} d_L$ . The luminosity distance,  $d_L$ , is given by Eq. (5). The change in volume element affects the SNRs when expressed in units number of SNe per  $\text{Mpc}^3$  per yr. It does not, however, change the estimated rates of observed core collapse SNe expressed in number of SNe per square angle. This is due to the fact that the core collapse SNR is directly proportional the observed luminosity density of galaxies, which is calculated from the number of galaxies per redshift interval for a specific angle over the sky, an observational quantity independent of cosmology.

When it comes to the Type Ia SNe, the volume element enters the calculations since the time between the formation of the progenitor star and the explosion of the SN may be a significant fraction of the Hubble time. This dependency on cosmology increases as the delay time  $\tau$  increases. The general trend is an increased SNR for the alternative cosmologies at high redshift.

Fig. 9 show the estimated number per square arcmin of core collapse and Type Ia (using  $\tau = 1$  Gyr) SNe in the I and  $K'$  filters down to different limiting magnitudes for the three cosmologies, using the hierarchical model for star formation.

For the number of core collapse SNe the effect of changing cosmology is small for the reasons discussed above. Only at the very faintest magnitudes is there significant deviation between the models. At  $K' = 31$ , the estimated rates increase by a factor  $\sim 1.5$  when changing from SCDM to  $\Lambda$ CDM.

The estimated rates of Type Ia SNe differ at faint magnitudes by up to a factor two between the cosmologies. For  $\tau = 1$  Gyr the intrinsic rates of the OCDM and  $\Lambda$ CDM models are higher than the SCDM at redshifts  $z \gtrsim 1$ . It is, however, necessary to reach faint magnitudes ( $K' \sim 28$ ) to observe this increase

in the total rates. Note, however, that a Type Ia at peak magnitude has  $m \sim 25$  at  $z \sim 1$ . This means that using SNe seen at peak allows probing of the region where the rates start to differ between the cosmological models at more moderate limiting magnitudes. Ruiz-Lapuente & Canal (1998) discuss the use of Type Ia's to distinguish between different cosmologies. In Sect. 8 we comment on their results.

The increased Type Ia rates at high  $z$  for the alternative cosmologies means that the redshift cutoff moves to higher redshifts. This cutoff is also highly dependent on the delay time  $\tau$  (see Fig. 1). It is, however, somewhat less dependent on the SFR. Therefore, if  $\tau$  is known, it should be possible to constrain the cosmology, even if the SFR is not accurately known. As an illustration, including all SFR scenarios, and using  $\tau = 1$  Gyr ( $\tau = 3$  Gyr), results in a cutoff in the Type Ia rates at  $z \sim 2.5$ – $3.5$  ( $1.2$ – $1.5$ ) for the SCDM cosmology, while the drop is at  $z \sim 2.9$ – $4.9$  ( $1.6$ – $2.2$ ) and  $z \sim 3.2$ – $5.3$  ( $1.9$ – $2.6$ ) for the OCDM and  $\Lambda$ CDM cosmologies, respectively. The higher values in these redshift ranges correspond to the hierarchical star formation scenario.

## 6. Gravitational lensing

In a recent paper Marri & Ferrara (1998) study the effects of gravitational lensing (GL) on high- $z$  objects, in particular Type II SNe, for a hierarchical model of galaxy formation. For the three flat cosmologies they study (SCDM with  $\Omega_M = 1$ , LCDM with  $\Omega_M = 0.4$ ,  $\Omega_\Lambda = 0.6$  and CHDM with  $\Omega_M = 0.7$ ,  $\Omega_\nu = 0.3$ ), they find that there is at least a 10% chance that objects with  $z \geq 4$  are magnified by a factor  $\gtrsim 3$ . To estimate the effects of GL on our results we have therefore used their magnification probabilities on our model (i.e. their Figs. 4 and 5).

For the SCDM model, which yields the highest magnification, we find that the increase in the total number of core collapse SNe is only a few percent when using the NGST limits ( $M'_{AB} = 30.2$  and  $K'_{AB} = 31.4$ ). The effects are even smaller for the shorter wavelength bands. The reason for the small effect is that with the faint limits of the NGST almost all SNe up to  $z \sim 4$  are detected even without magnification, and that the number of SNe with even higher  $z$ , where the magnification has largest effect, is relatively small.

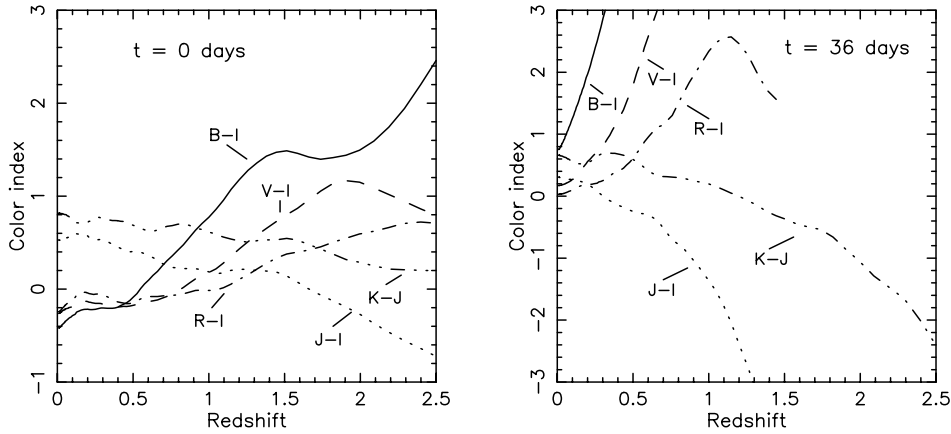


**Fig. 10.** Color indices for Type IIP SNe. The left panel shows indices at the peak, while the right panel shows indices at the plateau phase  $\sim 36$  days after the peak.

More interesting, for SNe with  $z \geq 4$  we find, when using the NGST  $M'$  limit, an increase by  $\sim 20\%$  of the predicted counts. For SNe with  $z \gtrsim 9$  the increase is  $\sim 40\%$ . It should, however, be noted that estimates presented by Porciani & Madau (1998) give a much lower probability for substantial magnification compared to the Marri & Ferrara results used in the estimates above. The reason for this seems to be that Marri & Ferrara assume point-like lenses, whereas Porciani & Madau use a more realistic mass distribution characterized by singular isothermal spheres. Therefore, the effects of gravitational lensing presented here could be overestimated.

## 7. Redshift determinations

A major problem when comparing predictions from different scenarios to observations is the determination of the SN redshift. A direct spectroscopic determination with a resolution of  $\gtrsim 100$  is only possible for SNe more than two magnitudes brighter than the limiting magnitude, i.e.  $I_{AB} \sim 25$  for 8–10 m class telescopes and  $K'_{AB} \sim 28.5$  for the NGST. To reach fainter magnitudes the main alternative is photometric redshifts of either the host galaxy or the SN. Photometric redshifts for galaxies have been discussed extensively by e.g., Fernández-Soto et al. (1999), Yee (1998), Gwyn (1995) and Connolly et al. (1995). The fact that a large fraction of the star formation up to  $z \gtrsim 1$  occurs in dwarf galaxies, as well as the cosmological dimming, can make such a determination difficult. An alternative is to estimate a photometric redshift directly from the SN. A problem here is that the SN spectrum changes with both type and epoch.

To examine this possibility we have determined broad band colors for the different types of SNe as function of epoch and redshift. As an example we show in Fig. 10 the color indices for a Type IIP SN as function of redshift at different phases. The spectra are taken from the synthetic spectra calculated by Eastman et al. (1994). These spectra assume LTE, but may nevertheless give a good impression of the qualitative evolution.

At early time, before  $\sim 20$  days the spectrum is a fairly smooth blackbody without a strong UV cutoff. The color indices do therefore not change dramatically with redshift. At

later stages in the plateau phase the spectrum does not change much. An important aspect is that the UV cutoff at  $\sim 4000 \text{ \AA}$  has now developed to its full extent, and the UV is essentially black. This is probably the most useful feature for identifying high redshift SNe photometrically. The extent of this UV drop may, as we discuss below, depend on the metallicity. The UV cutoff has a very pronounced effect on the optical color indices at  $z \lesssim 1$ , with strong increases in the B-I, V-I and R-I indices at successively larger  $z$ . For  $z \gtrsim 1$  the J-I and K-I, and finally K-J, are most useful due to the essential disappearance of the SNe in the optical.

A problem with photometric redshifts of SNe, compared to galaxies, is that the colors, as we have seen, depend sensitively on the epoch. In addition, they depend on SN type. E.g., Type IIL's have less UV blanketing, while the Type Ia's have a rapid development of the UV cutoff. To break this strong degeneracy it is essential to have information about both SN type and epoch. It is therefore necessary to obtain reasonable light curves, i.e. a fairly large number,  $\gtrsim 5-10$ , observations of the field. A complete analysis can therefore be quite costly in terms of observing time.

An alternative redshift method may be to use reasonably well sampled light curves in combination with the cosmic time dilation. For Type Ia SNe one can safely assume a standard light curve. Although the absolute luminosity can vary by a large factor, Type IIP's have a fairly well defined duration of the plateau phase, which lasts  $\sim 100$  days. Also Type IIL's and Ib's and Ic's have reasonably standardized light curves. From the observed light curve one can then, at least for SNe with  $z \gtrsim 1$ , get an approximate redshift within  $\sim 25\%$  from a comparison with the low  $z$  light curve templates. However, since the light curve should be followed over a decline of about  $\sim 2$  magnitudes in order to achieve a type specific light curve, the gain in depth by using photometry instead of multi object spectroscopy is marginal. The photometric accuracy also decreases for these levels and the actual limit may be even higher than two magnitudes. Therefore, in practice little is probably gained compared to direct spectroscopy.

## 8. Discussion

### 8.1. Uncertainties in the models

A major source of uncertainty is the treatment of dust extinction. In Sect. 4 we showed how different assumptions about the dust extinction affect the estimated rates. An underlying assumption in each of the calculations is that the same amount of dust affects the UV-luminosity from the high- $z$  galaxies (used to calculate the SNR) and the light from the SNe. If the UV-luminosity originates from regions with dust properties that differ considerably from the regions where the SNe originates, an extra dispersion in the estimated rates should be expected. It is, however, difficult to estimate the uncertainties in the rates introduced by this, since the distribution of the dust within the galaxies at high  $z$  is poorly known.

Other sources of uncertainties are the range of progenitor masses in Eq. (2) and the choice of IMF (Sect. 2.2), as well as the dependence on cosmology (Sect. 5). Also, the distribution of the different types among the core collapse SNe influences the estimates. Changes in the fractions of the faint SN1987A-like or bright Type II $n$ 's are most important. Due to their low luminosity, the SN1987A-like SNe will be too faint to be detected by ground based telescopes for  $z \gtrsim 0.5$  ( $I_{AB} \gtrsim 27$  at peak). Doubling the fraction of these SNe from 15% to 30%, or, at the other extreme, setting the fraction to zero, changes the total number of detected SNe by  $\pm 18\%$  at these redshifts. Changing the fraction of Type II $n$ 's has a slightly different effect. By increasing  $f(\text{II}n)$  from 2% to 4%, which is the upper limit proposed by Cappellaro et al. (1997), the total number of detected core collapse SNe at  $I_{AB} \sim 24$  increases by  $\sim 17\%$ . At these magnitudes it is mainly low redshift SNe in the steep part of the SFR curve that contribute, explaining the relative large effect. At fainter limiting magnitudes, an increasing fraction of normal luminosity SNe are detected at, and even beyond, the peak. The relative increase due to the Type II $n$ 's is therefore marginal. For  $I_{AB} = 27$  the number of SNe increases by  $\sim 4\%$  and for  $K'_{AB} \sim 31.4$  the number increases by  $\sim 1\%$ .

Adding the uncertainties, we find that the counts of core collapse SNe may vary by a factor more than two due to insufficiently known model parameters.

The estimated rates of Type Ia SNe are subjected to even larger uncertainties. Besides the factors which also affect the core collapse SNe, the rates of Type Ia's depend strongly on the assumed progenitor scenario, and are more dependent on cosmology. Also, the normalization at  $z=0$  introduces an additional uncertainty by a factor  $\sim 3$ . Considering this, it seems unlikely that counts of Type Ia's can be used to set any constraints on the model parameters. With additional information about the redshift distribution of the SNe it should, however, be possible to constrain either the progenitor life time or the cosmology. One of these parameters must, however, be independently determined, since there is a degeneracy between the both when it comes to the estimated redshift distribution of the SNe. To decrease the uncertainties involved, well defined searches of SNe at low redshift are highly desirable.

### 8.2. Dependence on metallicity

With increasing redshift the mean metallicity decreases, although the dispersion may be higher than at present. It is therefore interesting to discuss the consequences of a lower general metallicity.

For Type Ia SNe, Kobayashi et al. (1998) argue that for one of the most likely progenitor scenarios, based on super-soft X-ray binaries, the necessary condition for a Chandrasekhar mass explosion may not occur for a metallicity of  $Z \lesssim 0.1 Z_{\odot}$ , consistent with the decrease in the galactic [Fe/O] ratio at this metallicity. The physical reason can be traced to the peak in the opacity curve at  $\sim 10^5$  K, produced by iron. In the scenario by Kobayashi et al., this corresponds to a drop in the Type Ia rate at  $z \sim 1.2$ . At higher redshifts Type Ia explosions are inhibited, since  $[\text{Fe}/\text{H}] \lesssim -1$  here. Including the possibility of a dispersion in the evolution of the metallicity leads Kobayashi et al. to conclude that a cutoff in Type Ia rates should occur at  $z = 1-2$ . The Kobayashi et al. scenario should observationally be similar to the  $\tau = 3$  Gyr model, with a turn-on at  $z \sim 1.5$ . Because the life time in their model is  $\tau = 0.6$  Gyr, the peak in the SNR should occur at  $z \gtrsim 1$ , rather than at  $z \sim 0.7$ , as in the  $\tau = 3$  Gyr model.

For core collapse SNe a lower metallicity can have several effects. First, line blanketing in the UV may decrease somewhat for the Type IIP's. Since this is mainly an ionization effect, rather than an abundance effect, it is, however, likely that this effect is small. This is partly confirmed by the calculations by Eastman et al. (1994), who find only a marginal decrease of the UV blanketing as the metallicity is decreased from solar to a tenth of solar. For extremely low metallicity, like for Pop. III stars with  $Z \lesssim 10^{-2} Z_{\odot}$ , blanketing may, however, decrease significantly, although the Balmer jump will still be present.

Secondly, the relative fraction between different SN types may change. In particular, the number of blue, compact supergiant progenitors similar to Sanduleak  $-69^{\circ} 202$  may increase. This would then lead to a larger fraction of faint SN1987A like SNe, decreasing the number of observable core collapse SNe at high  $z$ . We emphasize that the exact reason for the blue progenitor of SN1987A is not fully understood (e.g., Woosley et al. 1999).

Finally, the mass loss process of the SN progenitor may depend on the metallicity. An example is the known decrease of the mass loss rate with decreasing metallicity for radiatively accelerated winds (e.g., Kudritzki et al. 1987). In the red supergiant phase dust driven mass loss may be less efficient (Salasnich et al. 1999). The importance of binary mass transfer may also depend on the metallicity. A change in the mass loss rate with metallicity would change the relative proportions between the different core collapse types. In particular, a decrease of the total mass lost is expected to lead to a decrease in the number of Type IIL, Ib and Ic SNe, while favoring Type IIP's. In addition, a less dense circumstellar medium could then lead to a decrease in the ionization by the circumstellar interaction, and stronger line blanketing for the Type IIL and II $n$ 's. Note, how-

ever, that the mass loss process even for local red supergiants in their final phase is poorly understood.

### 8.3. SNe as probes of star formation

With large ground-based telescopes, and especially with NGST, it should be possible to detect SNe up to high redshifts, and to estimate the rates of both core collapse and Type Ia SNe. We have shown that because the rate of core collapse SNe follows the SFR, it should be possible to use observed rates of these SNe to constrain the SFR. As we have seen, a major problem is the influence of dust extinction. In this respect we note that the NIR bands have the advantage of being less affected by dust extinction than the observed UV-luminosities. At high redshifts these bands correspond to the optical rest wavelength bands, and have therefore a factor of 2–3 lower extinction than the UV bands. Different star formation models may therefore better be tested by using the K and M bands. Reaching high redshifts ( $z \gtrsim 2$ ), corresponding to  $K'_{AB} \gtrsim 27$ , increases the differences in the predicted counts between the star formation models significantly (see Sect. 4.3).

The estimated difference in the redshift-integrated counts between the hierarchical star formation model and the high dust star formation model is a factor  $\gtrsim 2$ . This is about the same factor produced by the uncertainties in the modeling. It is therefore difficult to use these counts to probe star formation scenarios, unless the parameters involved are better known. What seems more feasible is to use redshift subsamples to constrain the shape of the SFR. As shown in Sect. 4.3, for models with a flat SFR at high  $z$ , we estimate a factor  $\sim 4$ –5 more SNe with  $z \gtrsim 4$ . A major problem here is to determine the redshifts of the SNe (see discussion in Sect. 7).

A further problem is if a large fraction of the star formation takes place in galaxies with very large extinction, like M 82 or Abell 220 with  $A_V \sim 5$ –10 magnitudes (instead of  $A_V \sim 1$ , as for our high dust model). The difference between the optical and UV extinction is then of less importance, leading to a decrease in the estimated differences between the models. A similar large extinction may be indicated by the results of the ISO observations of some deep fields (e.g., Flores et al. 1999). Far-IR observations is then the most reliable way of deriving the true star formation rate. An alternative is to use some other source tightly coupled to star formation, but not affected by dust absorption. If gamma-ray bursts are related to some class of core collapse SNe (e.g., Type Ic's), they may be such class of objects (Cen 1998). Also radio observations may be interesting in this respect.

### 8.4. SNe and nucleosynthesis

The study of the nucleosynthesis by direct observation of SNe is naturally affected by the same problem as the star formation rate. Unless the dust extinction can be determined reliably in an independent manner, the true number of SNe is difficult to derive. In addition to this, the metallicity yields for SNe of different masses is non-trivial to derive even at low redshifts (e.g.,

Fransson & Kozma 1999). Only for SN 1987A and a couple of other SNe has this become possible. The alternative to use theoretical yields from collapse calculations is obviously less satisfactory. The lower metallicity may also affect e.g. the mass loss processes, as discussed in Sect. 8.2. This may change both the progenitor structure and the upper and lower limits for the core collapse and Type Ia SNe, as well as the heavy element yields. In our view one of the most interesting goals for the observation of SNe at high redshift may be to observationally study the differences between the SNe in the early universe and those today.

### 8.5. Spacing between observations

An important aspect concerning the detection of SNe is the spacing in time between the observations. In order to detect the SN, the magnitude has to change appreciably. The interval is primarily dependent on the shape of the light curve. Near the peak, where the SN changes relatively fast, a comparatively short time is sufficient. This applies to searches where detection of SNe on the rising part of the light curve is the main objective (e.g., searches for Type Ia's for  $\Omega_0$ ). Core collapse SNe, which have a flatter decline of the light curve, need a longer spacing. This is especially true for the Type IIP's, which in the plateau phase decline by  $\lesssim 1$  mag. Unless a SN can be detected (against the host galaxy) with this precision it will be missed. The limiting magnitude of the search also affects the necessary spacing. A deeper search results in a higher mean  $z$  of the observed SNe. Due to the cosmic time dilatation, the light curves of these SNe are stretched in time, implying that a longer interval between two observations is needed,  $\sim 100(1+z)$  days. Therefore, in order to detect these SNe a deep observation with the VLT requires an interval of  $\gtrsim 100$  days, while a corresponding NGST observation requires approximately a years interval.

### 8.6. Comparison to other works

Apart from the studies by Pain et al. (1996), Madau et al. (1998a) and Chugai et al. (1999), which we have already commented on, there is a number of related investigations.

Marri & Ferrara (1998) have studied of the effects of gravitational lensing of high redshift SNe. Using a Press-Schechter formalism and gravitational ray-tracing, they determine the magnification probability as function of redshift for different cosmologies. We have already discussed the implications of their lensing results for our simulations in Sect. 6. Marri & Ferrara use these magnification probabilities to estimate the observed magnitudes at high redshift. The fact that there is a relatively large probability,  $\gtrsim 10\%$  for a factor of three or larger magnification for  $z \gtrsim 4$ , means that even SNe as distant as  $z \sim 10$  may be within the limits of NGST. When estimating the observed magnitudes they, however, assume that the light curve is described by a Type IIP light curve without any dispersion in magnitude, although as we have seen, the Type IIP's show a very large variation in luminosity. They also assume a fairly high temperature,  $\sim 25\,000$  K during the first 15 days, which

is twice as high as the models by Eastman et al. (1994) give. This is especially important for the high- $z$  SNe, and, as Marri & Ferrara show, a lower temperature makes the detectability considerably more difficult. Marri & Ferrara do not attempt any discussion of expected rates of the high- $z$  SNe.

The effects of gravitational lensing is also investigated by Porciani & Madau (1998). They find, as earlier mentioned, a considerably lower probability for a substantial magnification than Marri & Ferrara do. Porciani & Madau present I band counts for Type Ia and core collapse SNe, both including GL, and without lensing. These counts are presented as the number of SNe in different magnitude bins ( $21 < I_{AB} < 27$ ), seen at the peak of the light curve for an effective observation duration of one year. This leads to lower estimates for the observable number of SNe compared to our estimates, where we include SNe detected over the whole light curve. To compare our results we have calculated counts in the same units as used by Porciani & Madau. We find a fairly good agreement between the core collapse counts (deviation by a factor  $\sim 2$ ), but a somewhat worse agreement between the Type Ia counts. It should be noted that expressing rates in units of an effective observation duration requires an idealized observational procedure (as we have shown in the examples in Sect. 3.1).

Ruiz-Lapuente & Canal (1998) discuss the possibility of using R band counts of Type Ia SNe to distinguish different progenitor scenarios. They find, similar to our estimates, that models with long-lived progenitors result in higher counts than models with short-lived progenitors. To use this as a probe they note that it is necessary to know the SFR better than a factor 1.5. However, the uncertainty in the SFR seems, as we have shown, to be larger than this. It should therefore be difficult to use counts to determine progenitor scenarios. Additional information about the redshift distribution of the SNe is required.

The same authors also estimate the effects on the counts for alternative cosmologies. They find that a flat  $\Lambda$ -dominated universe ( $\Lambda$ CDM) should result in higher counts of Type Ia SNe than a standard cold dark matter universe (SCDM). The difference between the cosmologies start at  $m_R \sim 24$ , and increases at fainter limiting magnitudes. A somewhat smaller increase in the counts is found for an open universe with zero cosmological constant (OCDM).

Our results for different cosmologies agree with the general trend of Ruiz-Lapuente & Canal. Using counts to distinguish between cosmologies, however, requires both that the SFR is well known, and that restrictions can be set on the progenitor life time. If this is not the case, the degeneracy between the different parameters involved makes a distinction between cosmologies very difficult.

In an interesting paper Miralda-Escudé & Rees (1997) discuss the possible detection of very high redshift core collapse SNe at  $z \gtrsim 5$ . By requiring that a metallicity  $\sim 10^{-2} Z_{\odot}$  is produced at  $z \sim 5$ , they estimate a rate of about one core collapse SN per square arcmin per year above  $z \sim 5$ . Our extrapolated hierarchical model gives a rate of  $\sim 0.05$  SN per square arcmin per year above  $z \sim 5$ . This may favor models with a flat SFR at high  $z$ , which result in  $\sim 0.4$  (0.7) SNe per square arcmin

per year above  $z \sim 5$  when using  $z_F = 7$  ( $z_F = 10$ ). However, the metallicity used by Miralda-Escudé & Rees may be overestimated by an order of magnitude (Songaila 1997), leading to an overestimate of the SNR by the same amount. Also, the redshift before which the metallicity is assumed to have been produced affects the comparison. Using  $z \sim 3$ , instead of  $z \sim 5$ , decreases the estimated number SNe given by Miralda-Escudé & Rees by  $\sim 30\%$ . More important, integrating our rates for redshifts above  $z = 3$ , instead of  $z = 5$  as done above, results in a number of SNe that is a factor  $\sim 4$  higher. Other uncertainties in the estimate by Miralda-Escudé & Rees include the actual fraction of the baryonic matter which is enriched by the SNe.

Miralda-Escudé & Rees limit their discussion to Type IIP SNe, and do not attempt a detailed discussion of the observed rates. The observed magnitudes compare fairly well with our magnitudes in the K and M bands, but are brighter in the optical and near-IR bands. The main reasons for this is that they use a higher effective temperature and that they do not take into account any line blanketing in the UV, as our models do. As we discuss in next section, the low metallicity may decrease this effect. Apart from these caveats, the discussion by Miralda-Escudé & Rees provides an important constraint at high redshifts.

Gilliland et al. (1999) report on the discovery of two high redshift SNe in the HDF (see also Mannucci & Ferrara 1999). One of the SNe has a probable host galaxy at  $z \sim 0.95$  (spectroscopically determined) and is possibly a Type II, whereas the other SN has a probable host galaxy at  $z \sim 1.3$  (photometrically determined) and is likely a Type Ia. Gilliland et al. also make detailed estimates of the expected number of Type Ia and Type II SNe in a HDF like search. With limiting magnitude  $I_{AB} \sim 27.7$  they find that  $\sim 0.32$  Type Ia SNe should be detected in a search consisting of the HDF together with an observation of the same area made two years after the HDF. Using the same cosmological model as Gilliland et al. ( $\Omega_M = 0.28$ ,  $\Omega_{\Lambda} = 0.72$ ,  $H_0 = 63.3$  km/s/Mpc<sup>3</sup>) and  $\tau = 1$  Gyr, we estimate  $\sim 0.6$  Type Ia SNe for a similar search. For a flat  $\Omega_M = 1$  cosmology we estimate 0.7 SNe. The main reason for the difference in results is that Gilliland et al. use a constant Type Ia SNR over the redshift range of interest ( $0 < z \lesssim 1.5$ ), which is considerably lower than the mean value of our rates out to  $z \sim 1.5$ .

For Type II SNe Gilliland et al. estimate  $\sim 1.2$  SNe in HDF style search. This is in good agreement with our results, even though the modeling differs in many aspects. We estimate  $\sim 1.0$  core collapse SNe for the cosmology used by Gilliland et al., and 1.3 SNe for a  $\Omega_M = 1$  cosmology.

Considering the small statistics, both estimates are consistent with the discovery of two SNe in the HDF.

Sadat et al. (1998) discuss the cosmic star formation rate, using a spectrophotometric model for different assumptions of the dust extinction. From this they calculate SNIa and core collapse rates, but do not translate these into directly observable rates. Their SFR is a factor  $\gtrsim 3$  higher than ours, which seems mostly to be due to the use of different factors when converting the observed luminosity densities to the SFRs. This also leads to higher SNRs (their Fig. 2). Sadat et al. also presents a case for Type Ia rates with a different normalization. These rates (their

Fig. 3) agree better with our estimates at low redshifts. At high redshifts the Type Ia rates differ more due to different modeling of these SNe.

Jørgensen et al. (1997) attempt a calculation of the absolute rates of Type Ia, II and Ib SNe from a population model. Although in principle appealing, this model depends on the uncertain scenarios for the progenitors of especially the Type Ia's, as we have already discussed in this paper. Any estimates will therefore be sensitive to these assumptions. They also neglect the distinction between Type IIP's and Type IIL's, which most likely originate from different progenitors. Further, Jørgensen et al. assume in the calculation of the observed magnitudes in the different bands as function of redshift, that the spectrum is characterized by that at the peak. As we have discussed, the spectrum and luminosity vary strongly with time. The most serious deficiency is in our view their neglect of the magnitude variation, as given by the light curve, which as we have seen, changes the observed rates by large factors. Their estimates of the observed rates are therefore highly questionable.

## 9. Conclusions

Observations of high redshift SNe are of interest for several reasons. First of all, one has through these a direct probe of the nucleosynthesis and star formation of the universe. In practice, there are several obstacles for a quantitative study of these issues. The fact that a large fraction of the star formation, and thus the SNe, may be hidden within optically thick dust can make it difficult to determine the total SFR and SNR accurately. This is certainly true for the optical bands, where we have found that the predicted total number of core collapse SNe with  $z \lesssim 1.5$  is rather insensitive to the assumed star formation scenario, as long as the star formation is calculated to match the same observed luminosity densities, and the same extinction is assumed for the UV light from the galaxies and the SNe. Observations in the near-IR are less affected by this, and offers a clear advantage to the observations of the far-UV, as used for Lyman break objects. However, if a large fraction of the star formation occurs in highly obscured star burst galaxies, also the near-IR rates are severely affected. A further advantage of using SNe as star formation indicators is that they are insensitive to surface brightness selection effects. A complication when it comes to studying the nucleosynthesis is that the yields of the supernovae may vary with metallicity.

An important motivation for searches of SNe at high redshift is that one can from this type of observations learn something about the SNe themselves when observed in a different environment. In particular, differences in the fractions of the various core collapse subclasses, their spectra and luminosities may give new insight into the physics of the SNe and their progenitors.

The number of core collapse SNe that can be detected with NGST, with its expected limiting magnitude  $K' = 31.4$ , should be  $\sim 45$  per field in a  $10^4$  s exposure, assuming a hierarchical star formation scenario. The mean redshift of these SNe is  $\langle z \rangle = 1.9$ . About one third of the SNe have  $z \gtrsim 2$ . The high dust model results in total counts in the  $K'$  band that are a factor  $\sim 2$

higher than in the hierarchical model. The estimated number of SNe with  $z \gtrsim 2$  in the  $K'$  band for NGST is a factor  $\sim 3$  higher than in the hierarchical model. The model with flat SFR at high  $z$ , but with low extinction, result in a factor  $\sim 2$  higher number of SNe with  $z \gtrsim 2$ , compared to the hierarchical model, for the NGST limit.

An important practical point is that in order to detect especially the Type IIP SNe at high  $z$  it is necessary to have a spacing between observations of  $\sim 100$  days for ground based telescopes, and  $\sim 1$  year for deep observations with NGST. Shorter time intervals do not allow for the luminosity of the SNe to decrease by an amount necessary for detection.

When it comes to the observed rates of Type Ia SNe, we find that these are highly sensitive to the star formation modeling. This is due to the fact that the Type Ia's are less linked to the environment where their progenitors were formed. The uncertainty in the life-time of the progenitors, combined with the sensitivity of the Type Ia rates to the onset of star formation in the models with a flat SFR at high  $z$ , contributes to the difficulty with using Type Ia counts as probes for either different star formation scenarios or progenitor models. This is further hampered by the fact that even the local rate is highly uncertain, and that this propagates to other redshifts through the normalization of the rates at  $z = 0$ . Therefore, accurate measurements of the Type Ia rates at low  $z$  are most desired.

Precise measurements of the Type Ia rates at  $z \gtrsim 1$  could constrain the parameters to some extent. For example, in a given cosmology there is a high redshift cutoff in the Ia rates at an epoch that depends strongly on  $\tau$ , but is less dependent on the star formation scenario. In agreement with previous studies we find that counts of Type Ia SNe can be used as cosmological probes. This does, however, require that both the SFR and the unknown life time of the Type Ia progenitors can be determined independently.

We predict the number of simultaneously detectable Type Ia SNe per NGST field to be  $\sim 5$ –25, depending on progenitor model and star formation scenario. Additional uncertainties widen this range even more. Of the simultaneously observable Type Ia SNe, about 5% are on the rising part of the light curve. For a ground based telescopes with limiting magnitude  $I_{AB} \sim 27$  we predict 75–400 Type Ia's per square degree of which  $\sim 30\%$  are on the rise of the light curve.

A major technical aspect of our work is that we have tried to incorporate as much knowledge as possible about the theoretical and observational properties of the different classes of SNe. In particular, we have found that the spectral evolution is important for the magnitudes in the different bands. A striking example is the sensitivity to the UV cutoff, which for most SNe dominate the evolution in the optical bands. We have also found that a proper treatment of the light curve can change the predicted rates by factors of three or larger. An important source of uncertainty in these estimates are the local frequencies of SNe of different classes, as well as their distribution in luminosity. More extensive surveys with well defined selection criteria are therefore of highest priority for reliable predictions at high redshifts.

*Acknowledgements.* We are grateful to Claes-Ingvar Björnsson, Ariel Goobar, Bob Kirshner, Bruno Leibundgut, Ken Nomoto and Brian Schmidt for discussions, and especially to Ron Eastman for supplying their Type IIP results in digital form. This work is supported by the Swedish Natural Science Council and the Swedish Board for Space Sciences.

## References

- Blain A.W., Smail I., Ivison R.J., Kneib J.-P., 1999, *MNRAS* 302, 632
- Blinnikov S.I., Eastman R., Bartunov O.S., Popolitov V.A., Woosley S.E., 1998, *ApJ* 496, 454
- Branch D., Falk S.W., Uomoto A.K., et al., 1981, *ApJ* 244, 780
- Branch D., Lacy C.H., McCall M.L., et al., 1983, *ApJ* 270, 123
- Brinchmann J., Abraham R., Schade D., et al., 1998, *ApJ* 499, 112
- Burigana C., Danese L., De Zotti G., et al., 1997, *MNRAS* 287, L17
- Cappellaro E., Turatto M., Benetti S., et al., 1993, *A&A* 268, 472
- Cappellaro E., Turatto M., Fernley J., 1995, ESA Scientific Publication ESA-SP 1189
- Cappellaro E., Turatto M., Tsvetkov D.Y., et al., 1997, *A&A* 322, 431
- Cen R., 1998, *ApJ* 507, L131
- Chugai N., Blinnikov S., Lundqvist P., 1999, In: Cassisi S., Mazzali P. (eds.) *Future Directions in Supernova Research: Progenitors to Remnants*, in press
- Cole S., Aragon-Salamanca A., Frenk C.S., Navarro J. F., Zepf S.E., 1994, *MNRAS* 271, 781
- Connolly A.J., Csabai I., Szalay A.S., et al., 1995, *AJ* 110, 2655
- Connolly A.J., Szalay A.S., Dickinson M., Subbarao M.U., Brunner R.J., 1997, *ApJ* 486, L11
- Dahlén T., Fransson C., 1998, *The Next Generation Space Telescope: Science Drivers and Technological Challenges*. 34th Liège Astrophysics Colloquium, June 1998, p. 237
- Driver S.P., Fernández-Soto A., Couch W.J., et al., 1998, *ApJ* 496, L93
- Eastman R.G., Kirshner R.P., 1989, *ApJ* 347, 771
- Eastman R.G., Woosley S.E., Weaver T.A., Pinto P.A., 1994, *ApJ* 430, 300
- Ellingson E., Yee H.K.C., Bechtold J., Elston R., 1996, *ApJ* 466, L71
- Ellis R.S., Colless M., Broadhurst T., Heyl J., Glazebrook K., 1996, *MNRAS* 280, 235
- Evans R., Van Den Bergh S., McClure R.D., 1989, *ApJ* 345, 752
- Fernández-Soto A., Lanzetta K., Yahil A., 1999, *ApJ* 513, 34
- Filippenko A.V., 1997, *ARA&A* 35, 309
- Flores H., Hammer F., Thuan T.X., et al., 1999, *ApJ* 517, 148
- Fransson C., Kozma C., 1999, In: Phillips M., Suntzeff N. (eds.) *SN 1987A: Ten Years After, The Fifth CTIO/ESO/LCO Workshop*, in press
- Gilliland R.L., Nugent P.E., Phillips M.M., 1999, *ApJ* 521, 30
- Gordon K.D., Calzetti D., Witt A.N., 1997, *ApJ* 487, 625
- Gwyn S.D.J., 1995, MS Thesis, University of Victoria
- Hatano K., Branch D., Deaton J., 1998, *ApJ* 502, 177
- Hu E.M., Cowie L.L., McMahon R.G., 1998, *ApJ* 502, L99
- Hughes D.H., Serjeant S., Dunlop J., et al., 1998, *Nat* 394, 241
- Jørgensen H.E., Lipunov V.M., Panchenko I.E., Postnov K.A., Prokhorov M.E., 1997, *ApJ* 486, 110
- Kim A., Goobar A., Perlmutter S., 1996, *PASP* 108, 190
- Klein R.I., Chevalier R.A., Charles P., Bowyer S., 1979, *ApJ* 234, 566
- Kobayashi C., Tsujimoto T., Nomoto K., Hachisu I., Kato M., 1998, *ApJ* 503, L155
- Kudritzki R.P., Pauldrach A., Puls J., 1987, *A&A* 173, 293
- Larson R.B., 1974, *MNRAS* 166, 585
- Lilly S.J., Le Fevre O., Hammer F., Crampton D., 1996, *ApJ* 460, L1
- Lucy L.B., 1987, *A&A* 182, L31
- Madau P., Ferguson H.C., Dickinson M.E., et al., 1996, *MNRAS* 283, 1388
- Madau P., 1998, In: Livio M., Fall S.M., Madau P. (eds.) *The Hubble Deep Field: Proceedings of the Space Telescope Science Institute Symposium*, Baltimore, Maryland, May 6–9, 1997, Space Telescope Science Institute symposium series 11, Cambridge University Press, New York p. 200
- Madau P., Della Valle M., Panagia N., 1998a, *MNRAS* 297, L17
- Madau P., Pozzetti L., Dickinson M., 1998b, *ApJ* 498, 106
- Mannucci F., Ferrara A., 1999, *MNRAS* 305, 55
- Marri S., Ferrara A., 1998, *ApJ* 509, 43
- Meurer G.R., Heckman T.M., Lehnert M.D., Leitherer C., Lowenthal J., 1997, *AJ* 114, 54
- Miller D.L., Branch D., 1990, *AJ* 100, 530
- Miralda-Escudé J., Rees M.J., 1997, *ApJ* 478, L57
- Misner C.W., Thorne K.S., Wheeler J.A., 1973, *Gravitation*. W.H. Freeman and Co., San Francisco
- Nomoto K., 1984, *ApJ* 277, 791
- Nomoto K., Yamaoka H., Shigeyama T., Kumagai S. Tsujimoto T., 1994, In: Bludman S.A., Mochkovitch R., Zinn-Justin J. (eds.) *Supernovae*. Proc. LesHouches Session LIV, Elsevier Sci. Pub., p. 199
- Oke J.B., Gunn J.E., 1983, *ApJ* 266, 717
- Ortolani S., Renzini A., Gilmozzi R., et al., 1995, *Nat* 377, 701
- Pain R., Hook I., Deustua S., et al., 1996, *ApJ* 473, 356
- Panagia N., 1982, *European IUE Conference*, 31
- Pascarelle S., Lanzetta K., Fernández-Soto A., 1998, *ApJ* 508, L4
- Patat F., Barbon R., Cappellaro E., Turatto M., 1994, *A&A* 282, 731
- Pei Y.C., Fall S.M., Hauser M.G., 1998, *American Astronomical Society Meeting* 193, 4906
- Porciani C., Madau P., 1998, *ApJ*, submitted
- Pun C.S.J., Kirshner R.P., Sonneborn G., et al., 1995, *ApJS* 99, 223
- Riess A.G., Kirshner R.P., Schmidt B.P., et al., 1999, *AJ* 117, 707
- Rowan-Robinson M., Mann R.G., Oliver S.G., et al., 1997, *MNRAS* 289, 490
- Ruiz-Lapuente P., Canal R., 1998, *ApJ* 497, L57
- Sadat R., Blanchard A., Guiderdoni B., Silk J., 1998, *A&A* 331, L69
- Salasnich B., Bressan A., Chiosi C., 1999, *A&A* 342, 131
- Sawicki M., Yee H.K.C., 1998, *AJ* 115, 1329
- Schurmann S.R., 1983, *ApJ* 267, 779
- Smail I., Ivison R.J., Blain A.W., 1997, *ApJ* 490, L5
- Soifer B.T., Neugebauer G., Franx M., Matthews K., Illingworth G.D., 1998, *ApJ* 501, L171
- Somerville R.S., Primack J.R., 1998, In: *Proceedings of the Xth Rencontre de Blois*, June 1998, in press
- Songaila A., 1997, *ApJ* 490, L1
- Stockman H.S., 1997, In: Stockman H.S. (ed.) *Next Generation Space Telescope, Visiting a Time When Galaxies Were Young*. AURA, Inc.
- Tammann G.A., Loeffler W., Schroeder A., 1994, *ApJS* 92, 487
- Timmes F.X., Woosley S.E., Weaver T.A., 1995, *ApJS* 98, 617
- Timmes F.X., Woosley S.E., Weaver T.A., 1996, *ApJ* 457, 834
- Tsujimoto T., Yoshii Y., Nomoto K., et al., 1997, *ApJ* 483, 228
- Woosley S.E., Heger A., Weaver T.A., Langer N., 1999, In: Phillips M., Suntzeff N. (eds.) *SN 1987A: Ten Years After. The Fifth CTIO/ESO/LCO Workshop*, in press
- Yee H.K.C., 1998, In: *Proceedings of the Xth Rencontre de Blois*, June 1998, in press
- Yoshii Y., Tsujimoto T., Nomoto K., 1996, *ApJ* 462, 266
- Yungelson L., Livio M., 1998, *ApJ* 497, 168